HHS Public Access

Author manuscript

Neuron. Author manuscript; available in PMC 2019 December 19.

Published in final edited form as:

Neuron. 2018 December 19; 100(6): 1337–1353.e5. doi:10.1016/j.neuron.2018.10.031.

Complement C3aR inactivation attenuates tau pathology and reverses an immune network deregulated in tauopathy models and Alzheimer's disease

Alexandra Litvinchuk[1,2], **Ying-Wooi Wan**[3], **Dan B. Swartzlander**[1], **Fading Chen**[1], **Allysa Cole**[1], **Nicholas E. Propson**[1,4], **Qian Wang**[5], **Bin Zhang**[5], **Zhandong Liu**[6], and **Hui Zheng**[1,2,3,4,*]

[1]Huffington Center on Aging, Baylor College of Medicine, Houston, TX 77030, USA.

[2]Integrative Molecular and Biomedical Sciences Program, Baylor College of Medicine, Houston, TX 77030, USA

[3]Department of Molecular and Human Genetics, Baylor College of Medicine, Houston, TX 77030, USA

[4]Department of Molecular and Cellular Biology, Baylor College of Medicine, Houston, TX 77030, USA

[5]Department of Genetics and Genomics Science, Icahn Institute of Genomics and Multiscale Biology, Icahn School of Medicine at Mount Sinai, New York, NY10029, USA

[6]Department of Pediatrics-Neurology, Baylor College of Medicine, Houston, TX 77030, USA

SUMMARY

Strong evidence implicates the complement pathway as an important contributor to amyloid pathology in Alzheimer's disease (AD); however, the role of complement in tau modulation remains unclear. Here we show that the expression of *C3* and C3a receptor *(C3aR1)* are positively correlated with cognitive decline and Braak staging in human AD brains. Deletion of *C3ar1* in PS19 mice results in the rescue of tau pathology and attenuation of neuroinflammation, synaptic deficits, and neurodegeneration. Through RNA sequencing and cell type-specific transcriptomic analysis, we identify a C3aR-dependent transcription factor network that regulates a reactive glial switch whose inactivation ameliorates disease-associated microglia and neurotoxic astrocyte signatures. Strikingly, this C3aR network includes multiple genes linked to late-onset AD.

*Corresponding author and Lead Contact: Hui Zheng (huiz@bcm.edu).

AUTHOR CONTRIBUTIONS

A. L. and H.Z. designed the study; A.L. performed all in vitro assays and biochemical and immunohistochemical experiments and data analyses; Y-W.W. performed the bioinformatics analysis with input from A.L., D.S., H.Z. and Z.L.; D.S. made the differential gene expression heatmaps using RNAseq data; D.S., N.P and A.L. performed FACS-sorting experiments; F.C. performed the LTP recordings and analysis; A.C. performed behavioral tests and analysis; Q.W. and B.Z. performed the human-mouse correlation network analysis; A.L. and H.Z. wrote the paper. All authors provided input, read and approved the manuscript.

DECLARATION OF INTERESTS

The authors declare no competing financial interests.

Mechanistically we identify STAT3 as a direct target of C3-C3aR signaling that functionally mediates tau pathogenesis. All together our findings demonstrate a crucial role for activation of the C3-C3aR network in mediating neuroinflammation and tau pathology.

GraphicalAbstract

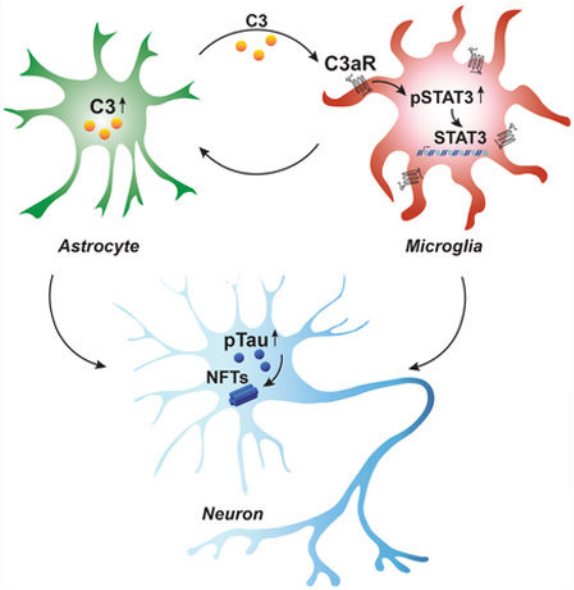

ETOC paragraph

Litvinchuk et al. show that complement C3aR plays a critical role in mediating immune homeostasis and tau pathology. The identification of a conserved C3aR network and crosstalk between complement signaling with STAT3 activation reveal novel pathogenic and therapeutic insights.

Keywords

Alzheimer’s disease; C3aR; Complement; Microglia; Neuroinflammation; STAT3; Tau

INTRODUCTION

Alzheimer’s disease (AD) is defined by the deposition of β-amyloid (Aβ) plaques and accumulation of neurofibrillary tangles (NFTs) in brains of diseased individuals. Besides the pathological hallmarks, AD is accompanied by prominent neuroinflammation, manifested by microgliosis, reactive astrogliosis, and elevated levels of proinflammatory cytokines (Heneka et al., 2015; Wyss-Coray and Rogers, 2012). Recent genetic studies provide strong support for a functional contribution of the innate immune response and microglia activation in late-onset AD (Efthymiou and Goate, 2017).

The complement pathway is a critical regulator of innate immunity (Veerhuis et al., 2011). Classical complement activation requires the cleavage of the central complement factor C3 to C3a and C3b, which elicit downstream events through binding to their receptors C3aR

and CR3, respectively (Stephan et al., 2012). The complement pathway molecules are expressed in the central nervous system (CNS) where they have been implicated in aging and disease processes. In particular, elevated C3 is detected in reactive astrocytes of both Aβ mouse models and AD brains (Lian et al., 2016; Liddelow et al., 2017). The C3-CR3 pathway promotes both early synapse loss (Hong et al., 2016) and age-associated cognitive decline in amyloid mouse models (Shi et al., 2017; Shi et al., 2015). Through an independent mechanism involving extracellular secretase activity, CR3 is shown to regulate Aβ degradation (Czirr et al., 2017). Besides the C3-CR3 pathway, signaling via C3-C3aR has also been implicated in various disease conditions, including viral-induced synapse loss and neurodegeneration in experimental lupus models (Jacob et al., 2010; Vasek et al., 2016). Relevant to AD, our previous studies reveal a C3-C3aR mediated neuron-immune crosstalk that influences network function and Aβ pathology (Lian et al., 2016; Lian et al., 2015), implicating a prominent role of the C3-C3aR axis in AD through intricate neuron-astrocyte-microglia interactions.

While the majority of studies in AD are focused on Aβ-associated effects, the role of the complement pathway in regard to tau pathology is less understood. Here, we examined the role of the C3-C3aR signaling on tau pathogenesis by crossing the PS19 tau transgenic animals with mice deficient in *C3ar1* (Humbles et al., 2000; Yoshiyama et al., 2007). Through neuropathological and functional determination and unbiased molecular interrogation, we reveal a critical role for C3aR in mediating an immune network and neuronal tau pathology. Further, our studies identify STAT3 as a direct target of C3aR that functionally regulate tau pathogenic processes.

RESULTS

C3 and *C3aR1* expression correlate with cognitive decline and Braak staging

To assess the impact of the complement C3-C3aR signaling in human disease, we first analyzed the *C3* and *C3aR1* expression using the reprocessed RNAseq data from the parahippocampal gyrus generated by the Mount Sinai School of Medicine Accelerating Medicine-AD consortium (Synapse ID: syn8484987). We observed an overall higher expression of *C3* and *C3aR1* with worsened cognitive function classified by no cognitive impairment (NCI), mild cognitive impairment (MCI), and dementia (Figure 1A and 1B) and with the degree of tau pathology stratified by Braak scores (Figures 1C and 1D). Quantitative real-time PCR (qPCR) analysis of *C3* and *C3aR1* mRNA levels in medial frontal cortices (MFC) of human tauopathy patients including corticobasal degeneration (CBD), Pick's disease (Picks), and progressive supranuclear palsy (PSP) also showed overall higher expression when compared to NCI controls (Figures 1E and 1F).

To determine whether a similar increase can be detected in mouse models of tauopathy, we measured *C3* and *C3ar1* mRNA levels in brain tissues (whole brain minus cerebellum) of PS19 tau transgenic mice, which overexpress mutant human P301S tau and develop neurofibrillary tangle-like pathology (NFTs), reactive gliosis, synapse and neuronal loss, and cognitive decline by 9 months of age (Yoshiyama et al., 2007). Although the expression levels of *C3* and *C3ar1* were comparable between PS19 mice and littermate wild-type (WT) controls at 4 months, their levels were significantly upregulated at 6 months and were further

elevated at 9 months (Figures 1G and 1H). Additionally we found that increased *C3* mRNA correlated with higher C3 protein levels (Fig.1I). Double immunostaining using anti-C3aR and anti-Ibal antibodies documented a high degree of co-localization and stronger intensity in the hippocampus of 9 month-old PS19 mice compared to WT controls (Figures 1J and 1K), indicating that increased C3aR expression in PS19 mice predominantly originates from microglia. The specificity of the anti-C3aR antibody was validated by its negative staining in *C3ar1* null mice (C3aR KO). Similar microglial staining of C3aR is also observed in MFC of AD and CBD brains (Figure S1). Combined, these data provide support for the activation of C3 and C3aR in human tauopathy diseases and tau transgenic mice.

C3ar1 ablation curtails neuroinflammation in aged PS19 mice

To investigate the role of C3-C3aR signaling in immune regulation and tau pathogenesis, we crossed the PS19 with C3aR KO mice and examined the neuroinflammatory profiles in the presence or absence of C3aR at 9 months of age (Figure 2). Immunostaining using anti-GFAP and anti-Ibal antibodies revealed marked increases in GFAP and Iba1 area fluorescence in PS19 mice (Figures 2A-2C). Strikingly, deletion of *C3ar1* on PS19 background almost completely normalized the GFAP and Iba1 immunoreactivity (Figures 2B and 2C, PS/KO vs WT, non-significant). Quantitative analysis of astrocyte and microglia morphologies using the Imaris software showed increased volumes and reduced branching and complexity in both cell types of PS19 mice, and these phenotypes were corrected by C3aR KO (Figure S2).

Complement C3 is highly expressed in reactive astrocytes where it marks the A1 neurotoxic sub-type implicated in AD and other neurodegenerative disorders (Lian et al., 2016; Liddelow et al., 2017). Consistent with the elevated *C3* mRNA and protein levels in 9 month-old PS19 mice (Figures 1G and 1I), we detected a drastic increase of C3 intensity in GFAP-positive astrocytes in PS19 mice that was almost completely abolished by *C3ar1* deletion (Figures 2D and 2E). This result was corroborated by the reduction of C3 protein levels in PS19/C3aR KO brains (Figure 2H). To further characterize the microglia phenotypes, we performed CD68 and Iba1 double staining to identify CD68-positive phagocytic microglia (Figure 2F). Quantification of CD68 immunoreactivity revealed that C3aR inactivation in PS19 mice significantly dampened the CD68 intensity in Iba1-positive microglia (Figure 2G). This result is supported by our earlier report showing that C3-C3aR signaling impinges on microglia phagocytosis (Lian et al., 2016). Finally, microglia and astrocyte activation is associated with increased production of pro-inflammatory cytokines including TNFα (Figure 2I), IL1 β (Figure 2J), and IL6 (Figure 2K). All three cytokines were elevated in brain tissues of PS19 mice, where inactivation of *C3ar1* resulted in a significant dampening of the cytokine levels. These results overall support the premise that C3aR regulates astrocyte and microglia reactivity and the production of pro-inflammatory cytokines in aged PS19 mice.

Genetic deletion of *C3ar1* attenuates tau pathology and improves neuronal function in tau transgenic mice

The above studies demonstrate a prominent role of C3aR in immune regulation. We next sought to assess the impact of C3aR loss-of-function on tau pathology and neuronal

function. Immunoblot analysis of PS19 and PS19/C3aR KO mice at 9 months of age using anti-phosphotau antibodies PHF1 and CP13 revealed a significant reduction of the hyperphosphorylated tau species in PS19/C3aR KO brains compared to the PS19 controls (Figures 3A and 3B). In contrast, total tau levels were not significantly changed between PS19 and PS19/C3aR KO mice, consistent with the comparable expression of human *MAPT* mRNA (Figure S3A). Thus, C3aR ablation results in the amelioration of pathological tau but not total tau. Remarkably, immunostaining using PHF1 (Figure 3C) and the confirmation-specific MC1 (Figure S3B) antibodies followed by quantification of PHF1- and MC1-positive neurons in the cortex and hippocampus revealed that *C3ar1* deletion resulted in an almost complete rescue of tau pathology (Figure 3D; Figure S3C).

To test the role of C3aR on learning and memory, we subjected WT, C3aR KO, PS19 and PS19/C3aR KO animals to the fear conditioning test at 8 months. We observed a reduction in contextual, but not cued fear response in PS19 mice, and a significant rescue in PS19/C3aR KO animals (Figure 3E), suggesting that C3aR KO is protective against the hippocampal-dependent memory impairment. To substantiate this finding, we performed LTP recordings of the Schaffer collateral pathway of the hippocampus from WT, C3aR KO, PS19, and PS19/C3aR KO mice. The LTP induction was significantly reduced in PS19 mice compared to WT and C3aR KO groups, and this phenotype was significantly improved in PS19/C3aR KO mice (Figure 3F). Combined, these data demonstrate that genetic deletion of *C3ar1* exerts beneficial effects on synaptic plasticity and cognitive function in PS19 mice.

C3aR inactivation rescues synapse and neuronal loss in PS19 mice

To further understand the functional rescue by C3aR loss, we examined the synaptic and neuronal properties of PS19 and PS19/C3aR KO mice along with WT and C3aR KO controls by high resolution imaging of synaptic marker proteins and unbiased stereology, respectively (Figure 4). Immunostaining of presynaptic protein synaptophysin (Syp) detected reduced intensity in the CA3 area of hippocampus of PS19 mice compared to WT and C3aR KO controls (Figure 4A). Deletion of *C3ar1* on PS19 background resulted in significant elevation of Syp immunoreactivity (Figures 4A and 4B). Similarly, co-immunostaining of Syp with postsynaptic marker PSD-95 revealed reduced pre-, post-, and double-positive synaptic puncta in PS19 mice, and the synapse loss was significantly restored by C3aR KO (Figures 4C and 4D; Figure S3D-S3G).

The complement pathway has been implicated in microglia-mediated synapse pruning (Hong et al., 2016; Vasek et al., 2016). Our earlier analysis showed higher intensity of CD68-positive phagocytic microglia in PS19 mice (Figure 2F), suggesting that reduced synaptic puncta seen in PS19 mice may be due to increased microglial engulfment. Indeed, measurement of the volume of Syp-positive (Figure 4E; Figure S3H) or PSD-95-positive (Figure S3I) puncta within Iba1-marked microglia, rendered by Imaris 3D imaging, revealed a negative association between total synaptic puncta and those inside the microglia in all genotypes (Figure 4F, compare with 4D; Figure S3J). The accumulation of cellular material in PS19 microglia, such as synapse, likely contribute to their augmented morphology (Figure S2).

In agreement with a previous report (Yoshiyama et al., 2007), unbiased stereology showed reduced neuronal numbers in both CA1 and CA3 areas of the hippocampus in 9-month-old PS19 mice (Figures 4G and 4H; Figures S3K and S3L). *C3ar1* ablation in PS19 mice led to a robust rescue of neurodegeneration, evidenced by the insignificant differences between PS19/C3aR KO and WT controls (Figure 4H).

C3aR controls the expression of an immune network conserved between human AD and PS19 mice

To gain a deeper understanding of the molecular mechanisms underlying C3aR function, we performed RNA sequencing (RNAseq) analysis of the hippocampal tissues of 9 month-old WT, C3aR KO, PS19, and PS19/C3aR KO mice. After removal of outliers identified by principal component analysis (PCA) (Figure S4A), we identified 1726 differentially expressed genes (DEGs, adjusted-$p<0.01$) in PS19 mice compared to WT controls, of which 1155 genes were upregulated and 571 downregulated (Figure S4B). Using unsupervised clustering analysis, we next examined the expression profiles of the 1726 DEGs across the four genotypes and found that the WT and C3aR KO are clustered together while the PS19/C3aR KO mice grouped in between PS19 and WT/C3aR KO animals (Figure 5A), indicating a partial rescue of PS19 DEGs by *C3ar1* deletion.

Further cross-genotype comparisons showed that although *C3ar1* knockout *per se* did not overtly perturb the global expression, with only 38 genes differentially expressed in C3aR KO vs WT (Figure 5B; Figure S4B), it resulted in the reversal of almost one-third of PS19 DEGs (526 out of 1726 PS19 DEGs were rescued) (Figure 5B). Indeed, comparison of PS19/C3aR KO to WT mice identified only 317 DEGs (137 up and 180 down, Figure S4B), implying that these two groups of animals are much closer in expression profiles than PS19 vs WT.

Interestingly, *C3ar1* deletion mainly rescued the expression of genes upregulated in PS19 mice (499 out of 526 genes, blue in upper left corner of Figure 5C) with only a small subset of the downregulated genes affected (27 out of 526, blue in lower right corner of Figure 5C). Gene Ontology (GO) analysis of the 1155 upregulated DEGs in PS19 mice revealed a significant upregulation of various immune pathway genes in PS19 mice, including the activation of innate and adaptive immunity, immune signaling, microglial activation, as well as pathways responsible for endosome-lysosome and vesicle formation (Figure 5D, upregulated genes in PS19 vs. WT). Importantly, all these categories were significantly rescued in PS19/C3aR KO mice (Figure 5D, downregulated genes in PS19/C3aR KO vs. PS19). Of the 27 downregulated genes that were rescued by C3aR KO, GO term analysis failed to reveal a significant enrichment of any particular pathways. Nevertheless, examination of the synaptic pathway genes observed a significant downregulation in PS19 mice (Figure S4C, PS19 vs WT). Although this is also the case in PS19/C3aR KO (Figure S4C, PS19/C3aR KO vs WT), the magnitude of the downregulated genes in PS19/C3aR KO mice was much milder compared to that of PS19 (180 vs 571 DEGs respectively). This result is consistent with the rescue of synaptic and neuronal loss by C3aR KO.

To assess the impact of the C3-C3aR signaling in human disease, we constructed a *C3aR1*-centered correlation network across eight human AD expression datasets from three studies

(Mount Sinai Brain Bank Studies BM10, 22, 36, 44 (Synapse ID: syn3157743); Harvard Brain Tissue Resource Study from PFC, VC, CR (Synapse ID: syn3159435); and Religious Orders Study and Memory and Aging Project (ROS-MAP) Study (Synapse ID: syn3219045)) and then intersected the network with the 526 genes rescued in PS19/C3aR KO group (Figure S5D). We observed a significant enrichment in the expression of these DEGs in at least five human datasets, indicating a high degree of consistency between the human datasets and mouse C3aR controlled gene network (Figure 5E). Of these, 301 genes positively correlated with *C3aR1* expression in the human AD datasets were found downregulated in PS19/C3aR KO mice (red circle in the network), seven were negatively correlated with *C3AR1* human AD database and upregulated in PS19/C3aR KO (blue circles in network), and only three were negatively correlated but not rescued in PS19/C3aR KO (pink circles in the network). These genes are enriched in the inflammatory response (GO: 0006954; Fisher Exact Test p=1.3E-17, 4.5 fold enrichment or FE) and immune cell activation (GO:0002263; Fisher Exact Test p=2.40E-15, 5.0 FE) pathways. Significantly, the network includes a group of genes linked to late-onset AD implicated in microglia activation: (*Abi3, Sall1, Spi1, Trem2*), immune response (*Bcl3, Gal3st4, Hla-Dqa1, Inpp5d, Lrrc25, Pycard, Sbno2*), and the complement pathway (*Clu, Ms4a6a*) (Efthymiou and Goate, 2017; Sims et al., 2017; Zhang et al., 2013). Together, these results provide support for conserved changes in the expression of C3aR-regulated gene signatures between mice and humans and indicate that the elevated C3-C3aR signaling may contribute to AD pathogenesis through regulating inflammatory response and immune cell activation.

C3aR inactivation reverses microglia and astrocyte gene signatures and a network of immune transcription factors in PS19 mice

Since microglia and astrocytes are the main cell types exerting the immune response in the brain, we performed gene set enrichment analyses (GSEA) for microglia sensome (Figure 6A; Figure S5A) and reactive astrocyte genes (Figure 6B; Figure S5B) (Hickman et al., 2013; Zamanian et al., 2012). We found that both gene sets were highly enriched in PS19 mice (Figures 6A and 6B, PS19 vs WT), and rescued almost to the same degree in PS19/C3aR KO animals (Figures 6A and 6B, PS19/C3aR KO vs PS19). Similar results were observed when GSEA was performed on complement pathway genes (Figure 6C; Figure S5C).

Changes in gene expression observed in the bulk brain may result from quantitative differences in cell numbers or qualitative alterations within a cell, or both. To distinguish these possibilities, we used a FACS-based concurrent brain cell-type acquisition (CoBrA) methodology (Swartzlander et al., 2018), and sorted microglia and astrocytes from 9 month-old mice to determine the cell-type specific gene expression (Figure S6A). Compared to WT and C3aR KO samples, microglia purified from PS19 mice produced higher levels of cytokines, chemokines, and complement pathway genes (Figure 6D). Of interest, the expression of disease-associated microglia (DAM) markers (Keren-Shaul et al., 2017), including *Axl, Csf1, Clec7a,* and *Itgax,* was greatly elevated in PS19 mice. Deletion of *C3ar1* in PS19 mice resulted in a significant reduction of all pro-inflammatory genes and DAM markers (Figure 6D, PS/KO). In contrast to the bulk brain result, we did not observe significant changes in *Aif1* or *Cd68* expression in purified microglia from PS19 mice

(Figure 6D), indicating that elevated *Aif1* expression in the bulk brain may be attributed by increased microglia numbers. This is supported by the higher percentage of Ki-67-positive Iba1-marked microglia in hippocampus of PS19 but not PS19/C3aR KO mice when compared to WT and C3aR KO animals (Figure S6B and S6C). Thus, the changes in microglia gene expression in PS19 mice are likely caused by increased cell number and activation status, phenotypes that are mitigated by *C3ar1* ablation.

Similar analysis of gene expression in purified astrocytes of the four groups of animals showed increased expression of *Gfap* and pan astrocyte markers *Aspg, Osmr, Serpina3n,* and *Cxcl10,* complement genes, and the recently described neurotoxic A1 astrocyte genes in PS19 mice (Liddelow et al., 2017). Interestingly, the A2 astrocyte genes were only partially affected (Figure 6E, PS19 A1 vs A2). *C3ar1* deletion significantly reduced the levels of complement and A1 astrocyte signatures (Figure 6E, PS/KO). Combined, these results indicate that C3aR confers its immune function through the regulation of key microglia and astrocyte gene expression profiles in PS19 mice.

The dramatic rescue of neuroinflammatory signatures in distinct cell subtypes by C3aR inactivation prompted us to speculate that C3aR may regulate the expression of key transcription factors (TFs) that drive the expression changes in PS19 mice. To test this hypothesis, we built a PS19 TF network based on the expression levels of DEGs between PS19 and WT mice using the TRANSFAC database (Figure 6F; Figure S7A) (Matys et al., 2006). We identified eleven TFs upregulated in PS19 mice that are implicated in mediating the inflammatory responses (*Stat1, Stat3, Stat5a, Stat5b, Nfkb1, Nfe2l2, Fli1*), microglia proliferation and differentiation (*Irf8, Spi1, Runx1*), and astrocyte maturation and neurogenesis (*Pax6*) (Ginhoux et al., 2010; Kierdorf et al., 2013; Zamanian et al., 2012; Zusso et al., 2012). Among these, the expression of five immune and inflammatory TFs, namely *Stat3, Nfe2I2, Irf8, Spi1,* and *Runx1* were significantly rescued by C3aR KO (Figure 6F, rescued TFs highlighted by red circle surrounding the upregulated genes), demonstrating a potent role of C3aR blockade in restricting microgliosis and dampening the neuroinflammation. These results were validated by qPCR analysis in an independent group of animals (Figure S7B). Interestingly, we observed similar upregulation of the TFs in human tauopathy brain samples (Figure S7C), indicating that the inflammatory and glial differentiation transcriptional programs are conserved in mouse and human tauopathy conditions.

To delineate the cell types that drive the TF changes detected in bulk brain samples, we performed qPCR analysis of FACS-sorted microglia and astrocytes from a separate cohort of 9 month-old mice. We found that the expression of all 11 TFs upregulated in PS19 mice can be readily detected in microglia preparations (Figure 6G), while only a subset (*Stat3, Stat5b, Nfkb1, Nfe2I2, Fli1 and Pax6*) were expressed in sorted astrocytes (Figure 6H), suggesting that microglia play a primary role in mediating the transcriptional changes in PS19 mice downstream of C3aR. This assessment is consistent with the microglial C3aR expression pattern in mouse brains (Figure 1J) and a robust rescue of microglia sensome gene expression in PS19/C3aR KO mice (Figure 6A; Figure S5A).

Direct induction of STAT3 signaling by C3-C3aR activation

The signal transducers and activators of transcription (STATs) represent a class of transcriptional factors involved in multiple cellular processes, particularly immune response (Shuai and Liu, 2003). The activation of the STAT pathway involves its phosphorylation and translocation to the nucleus where it mediates the transcription of target genes. Our TF network analysis revealed a group of STATs (*Stat1, Stat3, Stat5a,* and *Stat5b*) that were upregulated in PS19 mice (Figure 6F). Of these only *Stat3* expression was rescued by C3aR KO in bulk brain samples as well as in purified microglia (Figure 6G) and astrocytes (Figure 6H), indicating that STAT3 may be a specific target of C3aR. Indeed, independent proteomics analysis using the reverse-phase protein array (RPPA) platform identified total- and phospho-STAT3 (pY705) as a candidate upregulated in PS19 mice and subsequently rescued by C3aR KO (Figures 7A and 7B). These results were further confirmed by Western blot analysis of brain lysates (Figures 7C-7E), and corroborated by the appearance of nuclear pSTAT3 staining in astrocytes and microglia of aged PS19 mice (Figure S8A). Besides STAT3, only pRb, Beclin 1, and pNDGR1 were significantly changed in PS19 and PS19/C3aR KO samples (Figures S8B-S8D). In contrast, STAT5a was not altered across genotypes (Figure S8E).

Two possible mechanisms could contribute to the activation of pSTAT3 in PS19 mice and its downregulation by C3aR KO: One is through direct C3-C3aR signaling; the other is via the cytokine-induced canonical JAK-STAT pathway. Given the prominent microglial expression of C3aR, we sought to examine whether STAT3 can be activated by C3-C3aR in the BV2 microglia cell line and in primary microglia cultures. We first treated C3aR-overexpressing BV2 cells with IL6 or C3 and found that C3 induced STAT3 phosphorylation (Figure 7F) and nuclear translocation (Figures 7G and 7H) similar to IL6. These effects were effectively blocked by treating the cells with a C3aR antagonist (C3aRA) (Figures 7F-7H), demonstrating a direct regulation of the STAT3 pathway by C3aR. Next, to test if C3-C3aR induces the transcription of STAT3 target genes, we measured the STAT3 response element dependent luciferase activity and the expression of a well-established STAT3 target gene, the suppressor of cytokine signaling 3 (*SOCS3*) by qPCR. Consistent with the elevated pSTAT3 protein levels and its nuclear staining, we observed increased luciferase reporter activity (Figure 7I) and *SOCS3* mRNA levels (Figure 7J) in both IL6- and C3-treated cells, and the C3 effects were blocked by C3aRA. The direct regulation of pSTAT3 and its downstream signaling by C3-C3aR was also validated using primary microglial cultures derived from wild-type (Figures 7K and 7M) and *C3ar1* null (Figures 7L and 7N) mice. Specifically, while IL6-induced pSTAT3 and *SOCS3* expression in both WT and C3aR KO microglia (Figures 7K-7N, IL6), the C3-mediated pSTAT3 and *SOCS3* were only observed in WT (Figures 7K and 7M, C3), but not in *C3ar1*-deficient microglia (Figures 7L and 7N, C3). Additionally, C3-induced STAT3 phosphorylation and *SOCS3* expression were blunted by C3aRA in WT microglia (Figures 7K and 7M, C3/C3aRA). Together, these studies establish a novel signaling pathway that links C3-C3aR with STAT3 phosphorylation and activation.

Pharmacological inhibition of pSTAT3 mitigates tau pathology and neuroinflammation

The direct modulation of pSTAT3 activity by C3-C3aR signaling supports the premise that it may be the functional mediator downstream of C3aR. By extension, inhibition of pSTAT3 in

PS19 mice may confer a similar effect as C3aR ablation. To test this possibility, we resorted to a commercially available STAT3 phosphorylation site inhibitor SH-4-54 that was reported to cross the blood-brain barrier (Haftchenary et al., 2013). As expected, SH-4-54 (SH) effectively blocked the IL6- and C3-induced STAT3 phosphorylation (Figures S8F and S8G) and *SOCS3* expression (Figure S8H) in BV2 cells. We thus went on to assess its effect on tauopathy in vivo by treating the WT and PS19 mice with 10 mg/kg SH or vehicle (VC) three times a week beginning at 7 months for a total of 2 months. Compared to the PS19-VC group, SH-treated PS19 mice exhibited significantly lower pSTAT3 protein levels (Figure 8A and quantified in 8B) as well as *SOCS3* mRNA levels (Figure S8I). This is accompanied by reduced PHF1- and CP13-positive phospho-tau proteins (Figures 8A and 8B) and PHF1 (Figures 8C and 8D) and MC1 (Figures S8J and S8K) immunoreactivities in the hippocampus (HPC) and cortex (CTX) of PS19 mice.

Immunostaining analysis using antibodies against pSTAT3, GFAP, and Iba1 demonstrated a significant reduction of reactive astrogliosis and microgliosis as well as diminished pSTAT3 staining in the hippocampus of SH-treated PS19 mice (Figures 8E-8G). This result correlated with reduced levels of proinflammatory cytokines TNFα (Figure 8H), IL1 β (Figure 8I) and IL6 (Figure 8J) in SH-treated PS19 mouse brains. Combined, the direct activation of pSTAT3 signaling by C3-C3aR in vitro and the similar effects exerted by the blockade of C3aR or pSTAT3 in vivo provide support for a mechanistic and functional crosstalk between the complement and STAT3 signaling pathways in mediating tau pathogenic process.

DISCUSSION

Emerging evidence supports a pivotal role of innate immunity and neuroinflammation in AD and related disorders. In this study, we demonstrate that C3aR is a critical regulator of central immune homeostasis in the context of tau pathology. Genetic deletion of *C3ar1* leads to the attenuation of neuroinflammation, rescue of tau pathology, and amelioration of synaptic impairment and neuronal loss in PS19 mice. We identify a key immune transcription factor network that is subject to C3aR regulation and we reveal that pSTAT3 is a direct target of C3- C3aR signaling. Providing the relevance and significance of our findings to human disease, we document that the expression of *C3* and *C3aR1* are upregulated in human tauopathy brains and their levels are correlated with AD clinicopathology. Further, the C3aR-regulated network is highly conserved between humans and mice and constitutes immune and microglia factors implicated in late-onset AD.

Our RNAseq analysis revealed a significant upregulation of the inflammatory pathway genes in aged PS19 animals. Strikingly, genetic deletion of *C3ar1* normalized the expression of nearly half of the upregulated genes (499 out of 1156 genes) and reversed the DAM-microglia and A1 astrocyte phenotypes associated with neurodegenerative conditions (Keren-Shaul et al., 2017; Lian et al., 2016; Liddelow et al., 2017). The transcription factor analysis and cell-type specific molecular profiling suggest that these changes are driven by microglial proliferation and inflammatory gene expression programs. Combined with the predominant microglial C3aR expression and a significant rescue of microglia sensome, we posit that C3aR exerts its primary effect in PS19 mice through targeting the microglial

transcription factor network. Our results are in line with the previously reported crosstalk between the astroglial C3 and microglial C3aR and the notion that microglia activation triggers the induction of neurotoxic astrocytes marked by C3 (Lian et al., 2016; Liddelow et al., 2017).

Multiple mechanisms could contribute to the attenuation of tau pathology and improved synaptic and neuronal function in PS19/C3aR KO mice. First, the proinflammatory cytokines TNFα, IL1 β, and IL6 have been shown to promote tau phosphorylation in neurons (Bhaskar et al., 2010; Kitazawa et al., 2011; Quintanilla et al., 2004). Thus, the suppressed cytokine production in PS19/C3aR KO mice may curtail neuronal phospho-tau and associated pathology. Second, recent reports indicate that tau is secreted from neurons and can be taken up by microglia for degradation or transfer to other neurons (Asai et al., 2015; Bolos et al., 2016). Therefore, C3aR could influence tau/NFT pathology and neuronal and synaptic health through modulation of microglia-dependent tau and synaptic uptake. Last, the improved neuronal function may be directly attributed to the loss of neuronal C3aR as our previous studies uncovered a role of neuronal C3aR in modulating synaptic density and dendritic morphology through intraneuronal calcium and AMPA receptor trafficking (Lian et al., 2015). This idea gained further support by a recent report showing a detrimental effect of C3aR in promoting viral-induced synapse loss and cognitive decline (Vasek et al., 2016).

Mechanistically, we identify STAT3 as a downstream effector of C3aR; blocking this pathway with its phosphorylation inhibitor reduced neuroinflammation and partially rescued tau pathology in PS19 mice. The canonical STAT3 signaling involves cytokine-induced, Janus kinase (JAK)-dependent, STAT3 phosphorylation and nuclear translocation (Shuai and Liu, 2003). The complement molecules C3a and C5a have been shown to activate the canonical JAK-STAT3 signaling via cytokine intermediates in models of retinal and liver regeneration (Haynes et al., 2013; He et al., 2009; Strey et al., 2003). Although such an indirect mechanism could mediate C3aR-STAT3 interaction, here we establish a direct link between C3-C3aR signaling and STAT3 activation: C3 induces STAT3 phosphorylation, nuclear translocation, and *SOCS3* transcription in both BV2 cells and primary microglial cultures; these effects, but not IL6- induced STAT3 pathway, are abolished by C3aR antagonist treatment and in C3aR KO microglia. Besides the canonical JAK-dependent STAT phosphorylation, STAT3 can also be phosphorylated by other kinases, including Src and MAPK, through the activation of growth factor receptors and G-protein-coupled receptors (GPCR) (Mertens and Darnell, 2007; Ram and Iyengar, 2001). As a GPCR, it is plausible that C3aR may directly regulate STAT3 activity through G-protein signaling. However, the precise mechanism and the identity of the G-proteins remain to be established.

Although our in vitro studies are focused on microglial STAT3 signaling, it is important to note that strong evidence implicates a pivotal role of STAT3 in regulating astrogliosis and astrocyte reactivity in AD (Ceyzeriat et al., 2016). Indeed, increased *Stat3* mRNA and pSTAT3 staining are observed in both astrocytes and microglia of PS19 mice; these phenotypes are reversed by *C3ar1* deficiency and by STAT3 inhibitor treatment. In line with this assessment and extending beyond the tau/NFT pathogenesis, the STAT3 pathway is shown to be elevated in reactive astrocytes of Aβ mouse models where the expression of

SOCS3 effectively reduced reactive astrogliosis and microgliosis (Ben Haim et al., 2015). While the specific cell type was not defined, an independent study documented a role for the IL10-STAT3 pathway in mediating microglial Aβ phagocytosis (Guillot-Sestier et al., 2015). Overall, our data suggest that C3aR activates STAT3 signaling in astrocytes and microglia of PS19 mice through direct and indirect mechanisms. Additionally, given the complexity and the degree of crosstalk between the various immune pathways, other TFs such as members of STAT family (STAT1, STAT5a, and STAT5b), NF-κB, and NFE2L2 may work in parallel to augment the inflammatory responses in PS19 mice downstream of C3aR.

It is worth noting that our analysis is restricted to the resident immune cells in the CNS. C3aR is known to be widely expressed in the peripheral system, particularly upon inflammatory conditions. Our FACS analysis reveals the presence of low levels of infiltrating lymphocytes and monocytes in the brain (Figure S7), raising the possibility that C3aR in the periphery may impact the central immune system. Further studies using the *C3ar1* conditional allele are needed to decipher the central vs peripheral and cell-type specific effects of C3aR (Quell et al., 2017).

In conclusion, our studies establish a critical role of C3aR in mediating CNS immune homeostasis and tau pathology through targeting a transcription factor network that is highly conserved between tauopathy mice and human AD. We unveil a mechanistic and functional interaction between the C3-C3aR pathway and STAT3 signaling and provide novel insights for interrogating this pathway for therapeutic intervention.

STAR METHODS

CONTACT FOR REAGENT AND RESOURCE SHARING

Further information and requests for resources and reagents should be directed to and will be fulfilled by the Lead Contact, Dr. Hui Zheng (huiz@bcm.edu).

EXPERIMENTAL MODEL AND SUBJECT DETAILS

Mouse models.—The PS19 (IMSR_JAX:008169) and *C3art*-deficient (C3aR KO) (IMSR_JAX:005712) mice were obtained from the Jackson Laboratory. The C3aR KO mice were backcrossed to C57BL/6J for 5 generations prior to crossing with PS19 mice to obtain littermate WT, C3aR KO, PS19, and PS19/C3aR KO mice. Mice were housed 4-5 per cage in a pathogen free mouse facility with *ad libitum* access to food and water on a 12 hr light/dark cycle. Male and female mice at approximately equal ratio were used unless otherwise specified. All procedures were performed in accordance with NIH guidelines and approval of the Baylor College of Medicine Institutional Animal Care and Use Committee.

Cell cultures.—BV2 cells (CVCL_0182) were maintained in DMEM medium with 10% FBS (Blasi et al., 1990). Primary cultures were prepared as described previously (Lian et al., 2016). Briefly, mouse cortices and hippocampi were isolated from newborn pups in dissection medium (HBSS with 10 mM HEPES, 0.6% glucose, 1% v/v Pen/Strep) and cut into small pieces. Tissue was digested with 2.5% trypsin at 37°C for 15 min before trypsin inhibitor (1 mg/ml) was added. Tissue was centrifuged for 5 min at 1500 rpm, triturated, and resuspended in DMEM medium with 10% FBS. Cells were plated onto poly-D-lysine

(PDL)-coated T-75 flasks at 50,000 cells/cm^2 to generate mixed glial cultures. When confluent, microglia were separated by tapping the flasks against table and collecting the floating cells in media. Microglia cells were then seeded at 50,000 cells/cm^2 and cultured for another day in PDL-coated 12-well plates for protein/mRNA assays or on coverslips for staining.

Human subjects.—Postmortem brain tissues were provided by the University of Pennsylvania Center for Neurodegenerative Disease Research (CNDR). Informed consent was obtained from all subjects. The demographic data can be found in Table S2. Influence of sex, gender identity or both on the study results was not the objective of the study. It was not analyzed due to small sample size.

METHODS DETAILS

Mouse treatment.—STAT3 inhibitor (SH-4-54) was purchased from Apexbio (B4789) and prepared according to manufacturer ` s instructions. Briefly, SH-4-54 was solubilized in DMSO at 100 mg/ml and then diluted to 5 mg/ml in 50% PEG 4000 in PBS. Mice at seven months of age were treated with either SH-4–54 (10 mg/kg) or vehicle three times a week via i.p. injection for 2 months. Animals were sacrificed at 9 months of age for further analyses. A total of 8 mice/group was analyzed.

Cell treatment.—To induce pSTAT3 signaling, the BV2 cells or primary microglial cultures were first pre-treated with 10 mM C3aRA (Calbiochem, #SB290157) or 1 μM SH-4-54 (Apexbio, 4789) for 1 hr, then incubated with 50 ng/ml IL6 (R&D, 406-ML) or 10 μg/ml C3 (Millipore, #204885) for 1 hr for STAT3 nuclear localization experiments, 2 hrs for biochemical analysis, and 24 hrs to measure *SOCS3* mRNA expression.

STAT3 luciferase reporter assay.—First, we generated BV2 cells constitutively expressing *C3aR1.* Human *C3aR1* gene was amplified from pDNR-Lib-C3aR plasmid (Harvard Plasmid Database) and subcloned into FUGW vector (Addgene, 14883) (Lois et al., 2002). The lentivirus expressing *C3AR1* was packaged in HEK293T cells and harvested 48 hrs after transduction. To monitor STAT3 transcriptional activity, BV2 cells were transfected with the Cignal STAT3 Reporter (SABionsciences, CCS-9028L) using Lipofectamine 3000 (Thermofisher). 24 hours later, the transfected cells were treated with 50 ng/ml IL6 (R&D, 406-ML) or 10 μg/ml C3 (Millipore, #204885) for 24 hrs. The luciferase activity was measured using Promega Dual-Glo luciferase kit (E2920) according to manufacturer's instructions.

RNA extraction and quantitative PCR (qPCR).—Total RNA was extracted from cells or human or mouse brain tissues using RNeasy Mini kit (Qiagen, 74106). Reverse transcription was carried out using Superscript IV First Strand synthesis system (Invitrogen, 18091050). The qPCR analyses were performed using SYBR Green PCR master mix (Roche, 04673484001). Primer sequences can be found in Table S1.

Western blot analysis.—Tissues or cells were extracted in RIPA buffer supplemented with protease and phosphatase inhibitors (Roche, Complete Protease Inhibitor Cocktail,

04693116001 and Roche, PhosSTOP 049 06845001) and centrifuged at 15,000g for 20 min to collect the supernatant. Protein concentrations were determined using Pierce BCA Protein Assay (Thermofisher, 23225). Protein samples were diluted with 5xLaemmli buffer. After boiling, 8-10 μg of protein was loaded onto 10% SDS - polyacrylamide for protein separation. The membranes were then blocked with 5% milk in TBS/0.1% Tween - 20 (TBST) and probed with diluted primary antibody overnight at 4 °C (Rabbit anti-human tau (Dako, A0024), mouse anti- Stat3 (CST, 9139), rabbit anti-pStat3 (Tyr705) (CST, 9145), mouse anti- γ-tubulin (Sigma, T9026). Monoclonal PHF1 (pS396/pS404), CP13 (pS202/pT205), and conformational MC1 antibodies were gifts from P. Davies (Polydoro et al., 2009). Membranes were washed 3 × 10 min in TBST and blotted with secondary antibody (Horse anti-Rabbit-HRP, Vector Labs, 1:5000; Horse anti-Mouse-HRP, Vector Labs, 1:5000) for 1 hr at room temperature. The membranes were again washed 3 × 10 min in TBST, incubated in ECL solution (Pierce ECL kit, 32009), and exposed to film.

The C3/C3a protein levels in the brain lysates was estimated using the mouse C3 ELISA kit (Genway, #GWB-7555C7). The levels of TNFα, IL1 β, and IL6 were determined using DuoSet ELISA Kits from R&D (DY410, DY401, DY406) according to the manufacturer $ s instructions.

Immunostaining and image analysis.—After perfusion with 4% PFA, mouse brains were fixed with 4% PFA overnight at 4°C and then transferred i nto 30% sucrose solution. Brain sections (30 μm) were cut on a sliding microtome and stored at −20 °C in cryoprotectant. For each experiment, 5-6 corresponding sections were collected from 6-8 animals/genotype-treatment. After washing in TBS, sections or cultured cells on coverslips were blocked with TBS-T (0.4% Triton X-100) containing 2% donkey serum for 30 min, and then incubated in primary antibody diluted in blocking solution overnight at 4°C (mouse anti-GFAP (Millipore, AB_94844); rabbit anti- Iba1 (Wako, AB_839504); mouse anti-NeuN (Millipore, AB_2298772), rabbit anti-synaptophysin (Abcam, AB_2286949); rat anti-C3 (Hycult, AB_10129042); rat anti-C3aR (Hycult, AB_10130173); rabbit anti-pSTAT3 (Tyr705) (CST, AB_2491009)). For the pSTAT3 staining, sections or fixed cultures on coverslips were permeabilized with methanol for 10 min at −20°C prior to staining. After washing, the sections or coverslips were incubated with secondary antibodies for 1-2 hrs at room temperature and mounted in DAPI solution after final wash. DAB staining was carried out using VECTASTAIN Elite ABC Kit (PK-6200) following the manufacturer's instructions.

Human brain tissue sections were de-paraffinized in xylene and ethanol, boiled in citrate buffer (10mM Sodium Citrate, pH 6) for 10 min, and permeabilized in TBS-T solution for 15 min at room temperature. The sections were then stained with primary antibodies (mouse anti-C3aR (Hycult, HM2195), goat anti-mouse Iba1 (Abcam, ab48004), rabbit anti-human Tau T231 (Abcam, ab151559) diluted in blocking solution for 48 hrs at 4°C, and washed and stained with the appropriate secondary antibodies for 4 hrs prior to washing and mounting. The lipofuscin autofluorescence was quenched with the TrueBlack Lipofuscin Autofluorescence Quencher (Biotum, 23007) according to the manufacturer ` s instructions.

Brain sections or fixed primary cell cultures were imaged using a Leica TCS laser confocal microscope. For quantification of reactive glial cells and NFT load in the mouse cortex and hippocampus, sections were scanned using an EVOS FL Auto system. Images were then processed by ImageJ and background was subtracted by the software for fluorescence images before quantification.

Glial cell morphology quantification.—To quantify the glial cell morphology, Iba1-positive microglia and GFAP-positive astrocytes were imaged with a 63x oil objective using the confocal microscope with 0.2 μm step. Image background was subtracted using ImageJ and glial cell morphology were analyzed using the Bitplane Imaris software and Filaments option.

Synaptic imaging and quantification.—Synaptic puncta colocalization was quantified as previously described (Hong et al., 2016). Briefly, brain sections were co-immunostained with the anti-synaptophysin and anti-PSD-95 antibodies and imaged with the 63x objective oil with the 8x zoom using confocal microscopy with 0.2 μm step. Image background was subtracted using ImageJ, and the number of colocolized puncta was estimated using the Imaris software Bitplane Spots function with the Colocalize Spots Mat Lab script.

Quantification of synaptophysin inside microglia was performed as previously described using Imaris software (Schafer et al., 2014). Briefly, brain sections were co-immunostained with the anti-synaptophysin and anti-Iba1 antibodies, sections were imaged with the 63x objective oil with the 4x zoom using Leica confocal microscope with the 0.2 μm step. Image background was subtracted using ImageJ, and microglia and synaptophysin volumes were reconstructed using IMARIS software by Bitplane Surface function.

Unbiased stereology.—To estimate neuronal numbers in the CA1 and CA3 areas of hippocampus, brain sections from 9 month-old mice were immunohistochemically stained using the NeuN antibody and VECTASTAIN Elite ABC Kit (PK-6200) following the manufacturer's instructions. The number of neurons was counted from three 30 μm thick cryostat sections (every 6^{th} section) from bregma region between 2.58 and 1.62 mm lateral from the midline in one hemisphere of the mouse brain, according to the stereotaxic coordinates of mouse brain atlas (Franklin and Paxinos, 2001) using Stereo Investigator software by MBF Bioscience.

Cell-type purification and FACS sorting.—Mice were perfused with ice-cold PBS, adult mouse brains (whole brain minus cerebellum) were minced and resuspended in 2.5 mls of HBSS w/o Ca^{2+}, and w/o Mg^{2+} containing activated papain and DNase. Brains were incubated at 37° with gentle rocking for 15 minutes, then triturated 4 times with a fire-polished glass Pasteur pipet, and further dissociated with gentle rocking for an additional 15 minutes at 37°C. Following dissociation samples were mixed with HBSS+ (HBSS + 0.5% BSA, 2mM EDTA) and centrifuged for 5 min at 300g at 4°. After centrifugation the pellet was resuspended in 1000 μl of HBSS+, triturated 3 more times, and centrifuged for 15 seconds at 100g at room temperature. The supernatant was collected into a separate 15ml conical tube and this procedure was repeated 4 more times until all pelleted material was dissociated into single cells. Next, the supernatant was filtered through 40 μm cell strainer

(BD SKU 352340) and centrifuged for 5 min at 300g at 4°C. To remove myelin, the Miltenyi myelin removal beads were used according to the manufacturer ` s instructions (Miltenyi, 130-096-733). Briefly, the pellet was mixed with the beads in HBSS+ and incubated for 15 min at 4°C. After that, cells were washed in HBSS+ and centrifuged at 300xG for 5 min at 4°C. Next, the ce lls were resuspended in 1ml HBSS+ solution and passed through an LS column. The total effluent was then centrifuged for 5 min at 300g at 4°C to pellet the cells. For the antibody staining, the cells were resuspended in HBSS+ solution, blocked with FC block (BD, 553142), and then stained for 30 min with CD45-BV421 (BD, 563890), CD11b-FITC (BD, 553310) for microglia, ACSA-2-APC (Miltenyi, 130-102-315) for astrocytes, and cell viability blue fluorescent dye (Invitrogen, L23105). After FACS sorting, the cells were collected in 1.5 ml Eppendorf tubes, centrifuged at 1500 rpm for 5 min, and resuspended in RLT buffer containing 1% BME for future qPCR analysis. The mRNA was extracted using the Qiagen RNAEasy Micro kit (Qiagen, 74004).

RNAseq and analysis.—Total RNA from hippocampi of 9 month-old male mice was extracted using RNeasy Mini kit. The RNAseq analysis was performed using Illumina HiSeq2000 machine with the depth of 50-55 million pairs of reads per sample. Five 9 month-old male mice per genotype (total of 20 mice) were analyzed. Raw reads were first aligned to the *Mus musculus* genome (UCSC mm10) using TopHat v2.0.9 with default parameters (-r 100 –p 8) (Kim et al., 2013). The gene model was obtained from https://ccb.jhu.edu/software/tophat/igenomes.shtml. Then, htseq-count function of HTSeq was used to accumulate the number of aligned reads that fall under the exons of the gene (union of all the exons of the gene) to present the expression of each gene. Based on RNA expression levels, 3 outliers (AL2, AL15 and AL16) were removed after PCA analysis (Figure S2A) (Love et al., 2014). Differential gene analysis was carried out using the DESeq2 package in the R environment (Love et al., 2014). Differentially expressed genes (DEGs) were identified with the false-discovery rate (FDR) of 1%. Gene Ontology (GO) analysis was performed using DAVID (https://david-d.ncifcrf.gov/) on the mouse genome. The gene set enrichment analysis (GSEA) was performed using the ranked list of genes based on the log-fold change obtained from the differential gene analysis (Mootha et al., 2003; Subramanian et al., 2005). Transcription factor network analysis was conducted using the TRANScription FACtor database (TRANSFAC, release 2017.2) by extracting interactions of significant DEGs observed from RNASeq analysis and overlaying the changes of expression patterns to the network.

Human gene expression and correlation network analyses.—The expression levels of *C3* and *C3aR1* were obtained from Mount Sinai School of Medicine Study, AMP-AD RNAseq project, Synapse ID: syn8484987. Spearman's correlation coefficients were quantified to access the linear relationship between individual gene expression changes in parahippocampal gyrus of non-demented individuals (NCI, n=32) and patients diagnosed with mild cognitive impairment (MCI, n=34) or dementia (AD, n=160). To estimate the correlation of complement gene expression with tau pathology progression, the gene expression levels were stratified by Braak score I (n=24), II (n=34), III (n=37), IV (n=22), V (n=25), to VI (n=62); p-values were computed using AS 89 algorithm via the asymptotic t approximation implemented by the statistical package in R.

The *C3aR1* mouse-human correlation network was built using 8 datasets: Mount Sinai Brain Bank Studies BM10, 22, 36, 44 (Synapse ID: syn3157743); Harvard Brain Tissue Resource Study from PFC, VC, CR (Synapse ID: syn3159435); and Religious Orders Study and Memory and Aging Project (ROS-MAP) Study (Synapse ID: syn3219045). The correlation between *C3AR1* and all other genes was calculated based on gene expression level in each individual dataset. Gene expression levels measured in multiple probes within a dataset were represented by the probe with the largest variation in expression. The gene correlation with a Benjamini-Hochberg (BH)-corrected p-value<0.05 was considered significant. Fisher's Exact Test (FET) was performed to test for the enrichment between PS19/C3aR1 KO DEG signatures and *C3AR1*-correlated genes that were consensus across multiple human datasets.

Reverse phase protein array (RPPA).—For RPPA analysis, mouse brains (whole brain minus cerebellum) were first extracted in RIPA buffer and diluted to 1 μg/ml. The protein expression levels for 242 different antibodies (cancer panel) were determined using the Core Facility at MD Anderson Cancer Center (https://www.mdanderson.org/research/research-resources/corefacilities/functional-proteomics-rppa-core.html). A total of 64 samples, 7-10 mice per group at the age of 4 (data not shown) and 9 months were analyzed. 3 outliers from PS19 and PS19/C3aR KO group were removed from the analysis due to low detection signal.

Behavioral analysis.—Fear conditioning test was performed as described previously (Guo et al., 2013). Briefly, on the first day of the training each mouse was placed into the sound-attenuated chamber and allowed to explore for 2 min before a 75 dB white noise (conditioned stimulus) was presented for 30 sec followed by a 1.0 mA electric footshock (unconditioned stimulus) for 2 sec. The training was repeated one more time with a 2 min interval before mice were returned to the home cages. 24 hrs later the animals were placed in the same chamber for 5 min for a contextual fear conditioning response. For the cued test the mice were placed into a new chamber and allowed to freely explore for 3 min and then were presented with the sound for 3 min. In each case the freezing time was recorded automatically using Coulbourn/Actimetrics FreezeFrame3 System. N=15-20 mice/group with mixed genders at 8 months of age were used.

Electrophysiology.—Field recordings of Schaffer collateral LTP was performed as described before (Lian et al., 2015). Briefly, brains were isolated from 8-9 month-old female mice and cut into 400 μM slices on a vibratome. Stimulation of Schaffer collaterals from the CA3 region was performed with bipolar electrodes, while borosilicate glass capillary pipettes filled with recording ACSF (resistances of 2–3.5 5Ω) were used to record field excitatory postsynaptic potentials (fEPSPs) in the CA1 region. Signals were amplified using a MultiClamp 700 B amplifier (Axon), digitized using a Digidata 1440A (Axon) with a 2 kHz low pass filter and a 3 Hz high pass filter, and then captured and stored using Clampex 10.4 software (Axon) for offline data analysis. The genotypes and treatment groups were blinded to the experimenter. For each experiment 14-20 sections from 4-6 animals/genotype were used.

QUANTIFICATION AND STATISTICAL ANALYSIS

All data were analyzed with GraphPad Prism v.7 and presented as mean ± s.e.m. (*p<0.05, **p<0.01, and ***p<0.001). For simple comparisons, Student ` s t-test was used. For multiple comparisons ANOVA followed by the appropriate *post hoc* testing was utilized and is specified for each experiment in the figure legend. The statistical tests used for human data expression analyses are specified in the human data analysis methods section. All samples or animals were included in the statistical analysis unless otherwise specified.

DATA AND SOFTWARE AVAILABILITY

The RNAseq data has been deposited to NCBI's Gene Expression Omnibus (Accession Number GSE114910). Human expression datasets analyzed in the current study are available from AMP-AD portal upon registration (http://dx.doi.org/10.7303/syn2580853).

Supplementary Material

Refer to Web version on PubMed Central for supplementary material.

ACKNOWLEDGEMENTS

We thank Bianca Contreras and Nadia Aithmitti for expert technical assistance. We are grateful to Drs. John Trojanowski and Virginia Lee for providing human brain tissues and Peter Davies for the gift of PHF1, CP13, and MC1 antibodies. We thank Drs. Wei Cao, Ben Deneen, Rituraj Pal, and Heidi Martini-Stoica for valuable suggestions and for proofreading the manuscript. We acknowledge the support from the Cytometry and Cell Sorting Core at Baylor College of Medicine, with funding from the NIH (P30 AI036211, P30 CA125123, and S10 RR024574), and the M.D. Anderson Functional Proteomics RPPA (NCI #CA16672) and Next Generation Sequencing (#RP120348 and #RP170002) core facilities. This work was supported by grants from the NIH (R01 NS093652, R01 AG020670, R01 AG057509, and RF1 AG054111 to HZ).

REFERENCES

Asai H, Ikezu S, Tsunoda S, Medalla M, Luebke J, Haydar T, Wolozin B, Butovsky O, Kugler S, and Ikezu T (2015). Depletion of microglia and inhibition of exosome synthesis halt tau propagation. Nature neuroscience 18, 1584–1593. [PubMed: 26436904]

Ben Haim L, Ceyzeriat K, Carrillo-de Sauvage MA, Aubry F, Auregan G, Guillermier M, Ruiz M, Petit F, Houitte D, Faivre E, et al. (2015). The JAK/STAT3 pathway is a common inducer of astrocyte reactivity in Alzheimer's and Huntington's diseases. The Journal of neuroscience : the official journal of the Society for Neuroscience 35, 2817–2829. [PubMed: 25673868]

Bhaskar K, Konerth M, Kokiko-Cochran ON, Cardona A, Ransohoff RM, and Lamb BT (2010). Rw. Neuron 68, 19–31. [PubMed: 20920788]

Blasi E, Barluzzi R, Bocchini V, Mazzolla R, and Bistoni F (1990). Immortalization of murine microglial cells by a v-raf/v-myc carrying retrovirus. Journal of neuroimmunology 27, 229–237. [PubMed: 2110186]

Bolos M, Llorens-Martin M, Jurado-Arjona J, Hernandez F, Rabano A, and Avila J (2016). Direct Evidence of Internalization of Tau by Microglia In Vitro and In Vivo. Journal of Alzheimer's disease : JAD 50, 77–87. [PubMed: 26638867]

Ceyzeriat K, Abjean L, Carrillo-de Sauvage MA, Ben Haim L, and Escartin C (2016). The complex STATes of astrocyte reactivity: How are they controlled by the JAK-STAT3 pathway? Neuroscience 330, 205–218. [PubMed: 27241943]

Czirr E, Castello NA, Mosher KI, Castellano JM, Hinkson IV, Lucin KM, Baeza-Raja B, Ryu JK, Li L, Farina SN, et al. (2017). Microglial complement receptor 3 regulates brain Abeta levels through secreted proteolytic activity. The Journal of experimental medicine 214, 1081–1092. [PubMed: 28298456]

Efthymiou AG, and Goate AM (2017). Late onset Alzheimer's disease genetics implicates microglial pathways in disease risk. Molecular neurodegeneration 12, 43. [PubMed: 28549481]

Franklin KBJ, and Paxinos G (2001). The Mouse Brain in Stereotaxic Coordinates, 2nd edn (Academic Press).

Ginhoux F, Greter M, Leboeuf M, Nandi S, See P, Gokhan S, Mehler MF, Conway SJ, Ng LG, Stanley ER, et al. (2010). Fate mapping analysis reveals that adult microglia derive from primitive macrophages. Science 330, 841–845. [PubMed: 20966214]

Guillot-Sestier MV, Doty KR, Gate D, Rodriguez J, Jr., Leung BP, Rezai-Zadeh K, and Town T (2015). Il10 deficiency rebalances innate immunity to mitigate Alzheimer-like pathology. Neuron 85, 534–548. [PubMed: 25619654]

Guo Q, Li H, Cole AL, Hur JY, Li Y, and Zheng H (2013). Modeling Alzheimer's Disease in mouse without mutant protein overexpression: cooperative and independent effects of Abeta and tau. PloS one 8, e80706. [PubMed: 24278307]

Haftchenary S, Luchman HA, Jouk AO, Veloso AJ, Page BD, Cheng XR, Dawson SS, Grinshtein N, Shahani VM, Kerman KV et al. (2013). Potent Targeting of the STAT3 Protein in Brain Cancer Stem Cells: A Promising Route for Treating Glioblastoma. ACS medicinal chemistry letters 4, 1102–1107. [PubMed: 24900612]

Haynes T, Luz-Madrigal A, Reis ES, Echeverri Ruiz NP, Grajales-Esquivel E, Tzekou A, Tsonis PA, Lambris JD, and Del Rio-Tsonis K (2013). Complement anaphylatoxin C3a is a potent inducer of embryonic chick retina regeneration. Nature communications 4, 2312.

He S, Atkinson C, Qiao F, Cianflone K, Chen X, and Tomlinson S (2009). A complement-dependent balance between hepatic ischemia/reperfusion injury and liver regeneration in mice. The Journal of clinical investigation 119, 2304–2316. [PubMed: 19620784]

Heneka MT, Carson MJ, El Khoury J, Landreth GE, Brosseron F, Feinstein DL, Jacobs AH, Wyss-Coray T, Vitorica J, Ransohoff RM, et al. (2015). Neuroinflammation in Alzheimer's disease. The Lancet Neurology 14, 388–405. [PubMed: 25792098]

Hickman SE, Kingery ND, Ohsumi TK, Borowsky ML, Wang LC, Means TK, and El Khoury J (2013). The microglial sensome revealed by direct RNA sequencing. Nature neuroscience 16, 1896–1905. [PubMed: 24162652]

Hong S, Beja-Glasser VF, Nfonoyim BM, Frouin A, Li S, Ramakrishnan S, Merry KM, Shi Q, Rosenthal A, Barres BA, et al. (2016). Complement and microglia mediate early synapse loss in Alzheimer mouse models. Science 352, 712–716. [PubMed: 27033548]

Humbles AA, Lu B, Nilsson CA, Lilly C, Israel E, Fujiwara Y, Gerard NP, and Gerard C (2000). A role for the C3a anaphylatoxin receptor in the effector phase of asthma. Nature 406, 998–1001. [PubMed: 10984054]

Jacob A, Bao L, Brorson J, Quigg RJ, and Alexander JJ (2010). C3aR inhibition reduces neurodegeneration in experimental lupus. Lupus 19, 73–82. [PubMed: 19900981]

Keren-Shaul H, Spinrad A, Weiner A, Matcovitch-Natan O, Dvir-Szternfeld R, Ulland TK, David E, Baruch K, Lara-Astaiso D, Toth BV et al. (2017). A Unique Microglia Type Associated with Restricting Development of Alzheimer's Disease. Cell 169, 1276–1290 e1217. [PubMed: 28602351]

Kierdorf K, Erny D, Goldmann T, Sander V, Schulz C, Perdiguero EG, Wieghofer P, Heinrich A, Riemke P, Holscher, C_V et al. (2013). Microglia emerge from erythromyeloid precursors via Pu.1- and Irf8-dependent pathways. Nature neuroscience 16, 273–280. [PubMed: 23334579] $_V$

Kim D, Pertea G, Trapnell C, Pimentel H, Kelley R, and Salzberg SL (2013). TopHat2: accurate alignment of transcriptomes in the presence of insertions, deletions and gene fusions. Genome biology 14, R36. [PubMed: 23618408]

Kitazawa M, Cheng D, Tsukamoto MR, Koike MA, Wes PD, Vasilevko V, Cribbs DH, and LaFerla FM (2011). Blocking IL-1 signaling rescues cognition, attenuates tau pathology, and restores neuronal beta-catenin pathway function in an Alzheimer's disease model. Journal of immunology 187, 6539–6549.

Lian H, Litvinchuk A, Chiang AC, Aithmitti N, Jankowsky JL, and Zheng H (2016). Astrocyte-Microglia Cross Talk through Complement Activation Modulates Amyloid Pathology in Mouse

Models of Alzheimer's Disease. The Journal of neuroscience : the official journal of the Society for Neuroscience 36, 577–589. [PubMed: 26758846]

Lian H, Yang L, Cole A, Sun L, Chiang AC, Fowler SW, Shim DJ, Rodriguez-Rivera J, Taglialatela G, Jankowsky JL, et al. (2015). NFkappaB-activated astroglial release of complement C3 compromises neuronal morphology and function associated with Alzheimer's disease. Neuron 85, 101–115. [PubMed: 25533482]

Liddelow SA, Guttenplan KA, Clarke LE, Bennett FC, Bohlen CJ, Schirmer L, Bennett ML, Munch AE, Chung WS, Peterson TC, et al. (2017). Neurotoxic reactive astrocytes are induced by activated microglia. Nature 541, 481–487. [PubMed: 28099414]

Lois C, Hong EJ, Pease S, Brown EJ, and Baltimore D (2002). Germline transmission and tissue-specific expression of transgenes delivered by lentiviral vectors. Science 295, 868–872. [PubMed: 11786607]

Love MI, Huber W, and Anders S (2014). Moderated estimation of fold change and dispersion for RNA-seq data with DESeq2. Genome biology 15, 550. [PubMed: 25516281]

Matys V, Kel-Margoulis OV, Fricke E, Liebich I, Land S, Barre-Dirrie A, Reuter I, Chekmenev D, Krull M, Hornischer K, et al. (2006). TRANSFAC and its module TRANSCompel: transcriptional gene regulation in eukaryotes. Nucleic acids research 34, D108–110. [PubMed: 16381825]

Mertens C, and Darnell JE, Jr. (2007). SnapShot: JAK-STAT signaling. Cell 131, 612. [PubMed: 17981126]

Mootha VK, Lindgren CM, Eriksson KF, Subramanian A, Sihag S, Lehar J, Puigserver P, Carlsson E, Ridderstrale M, Laurila E, et al. (2003). PGC-1alpha-responsive genes involved in oxidative phosphorylation are coordinately downregulated in human diabetes. Nature genetics 34, 267–273. [PubMed: 12808457]

Polydoro M, Acker CM, Duff K, Castillo PE, and Davies P (2009). Age-dependent impairment of cognitive and synaptic function in the htau mouse model of tau pathology. The Journal of neuroscience : the official journal of the Society for Neuroscience 29, 10741–10749. [PubMed: 19710325]

Quell KM, Karsten CM, Kordowski A, Almeida LN, Briukhovetska D, Wiese AV, Sun J, Ender F, Antoniou K, Schroder T, et al. (2017). Monitoring C3aR Expression Using a Floxed tdTomato-C3aR Reporter Knock-in Mouse. Journal of immunology 199, 688–706.

Quintanilla RA, Orellana DI, Gonzalez-Billault C, and Maccioni RB (2004). Interleukin-6 induces Alzheimer-type phosphorylation of tau protein by deregulating the cdk5/p35 pathway. Experimental cell research 295, 245–257. [PubMed: 15051507]

Ram PT, and Iyengar R (2001). G protein coupled receptor signaling through the Src and Stat3 pathway: role in proliferation and transformation. Oncogene 20, 1601–1606. [PubMed: 11313907]

Schafer DP, Lehrman EK, Heller CT, and Stevens B (2014). An engulfment assay: a protocol to assess interactions between CNS phagocytes and neurons. Journal of visualized experiments : JoVE.

Shi Q, Chowdhury S, Ma R, Le KX, Hong S, Caldarone BJ, Stevens B, and Lemere CA (2017). Complement C3 deficiency protects against neurodegeneration in aged plaque-rich APP/PS1 mice. Science translational medicine 9.

Shi Q, Colodner KJ, Matousek SB, Merry K, Hong S, Kenison JE, Frost JL, Le KX, Li S, Dodart JC, et al. (2015). Complement C3-Deficient Mice Fail to Display Age-Related Hippocampal Decline. The Journal of neuroscience : the official journal of the Society for Neuroscience 35, 13029–13042. [PubMed: 26400934]

Shuai K, and Liu B (2003). Regulation of JAK-STAT signalling in the immune system. Nature reviews Immunology 3, 900–911.

Sims R, van der Lee SJ, Naj AC, Bellenguez C, Badarinarayan N, Jakobsdottir J, Kunkle BW, Boland A, Raybould R, Bis JC, et al. (2017). Rare coding variants in PLCG2, ABI3, and TREM2 implicate microglial-mediated innate immunity in Alzheimer's disease. Nature genetics 49, 1373–1384. [PubMed: 28714976]

Stephan AH, Barres BA, and Stevens B (2012). The complement system: an unexpected role in synaptic pruning during development and disease. Annual review of neuroscience 35, 369–389.

Strey CW, Markiewski M, Mastellos D, Tudoran R, Spruce LA, Greenbaum LE, and Lambris JD (2003). The proinflammatory mediators C3a and C5a are essential for liver regeneration. The Journal of experimental medicine 198, 913–923. [PubMed: 12975457]

Subramanian A, Tamayo P, Mootha VK, Mukherjee S, Ebert BL, Gillette MA, Paulovich A, Pomeroy SL, Golub TR, Lander ES, and Mesirov JP (2005). Gene set enrichment analysis: a knowledge-based approach for interpreting genome-wide expression profiles. Proceedings of the National Academy of Sciences of the United States of America 102, 15545–15550. [PubMed: 16199517]

Swartzlander DB, Propson NE, Roy ER, Saito T, Saido T, Wang B, and Zheng H (2018). Concurrent cell type-specific isolation and profiling of mouse brains in inflammation and Alzheimer's disease. JCI insight 3.

Vasek MJ, Garber C, Dorsey D, Durrant DM, Bollman B, Soung A, Yu J, Perez-Torres C, Frouin A, Wilton DK, et al. (2016). A complement-microglial axis drives synapse loss during virus-induced memory impairment. Nature 534, 538–543. [PubMed: 27337340]

Veerhuis R, Nielsen HM, and Tenner AJ (2011). Complement in the brain. Molecular immunology 48, 1592–1603. [PubMed: 21546088]

Wyss-Coray T, and Rogers J (2012). Inflammation in Alzheimer disease-a brief review of the basic science and clinical literature. Cold Spring Harbor perspectives in medicine 2, a006346. [PubMed: 22315714]

Yoshiyama Y, Higuchi M, Zhang B, Huang SM, Iwata N, Saido TC, Maeda J, Suhara T, Trojanowski JQ, and Lee VM (2007). Synapse loss and microglial activation precede tangles in a P301S tauopathy mouse model. Neuron 53, 337–351. [PubMed: 17270732]

Zamanian JL, Xu L, Foo LC, Nouri N, Zhou L, Giffard RG, and Barres BA (2012). Genomic analysis of reactive astrogliosis. The Journal of neuroscience : the official journal of the Society for Neuroscience 32, 6391–6410. [PubMed: 22553043]

Zhang B, Gaiteri C, Bodea LG, Wang Z, McElwee J, Podtelezhnikov AA, Zhang C, Xie T, Tran L, Dobrin Rv et al. (2013). Integrated systems approach identifies genetic nodes and networks in late-onset Alzheimer's disease. Cell 153, 707–720. [PubMed: 23622250]

Zusso M, Methot L, Lo R, Greenhalgh AD, David S, and Stifani S (2012). Regulation of postnatal forebrain amoeboid microglial cell proliferation and development by the transcription factor Runx1. The Journal of neuroscience : the official journal of the Society for Neuroscience 32, 11285–11298. [PubMed: 22895712]

Highlights

- Complement C3 and C3aR are activated in AD and tauopathy conditions
- C3aR inhibition reverses glial reactivity and rescues neuronal defects in PS19 mice
- C3aR controls an immune network conserved between mouse models and human AD
- STAT3 is a downstream target of C3-C3aR signaling

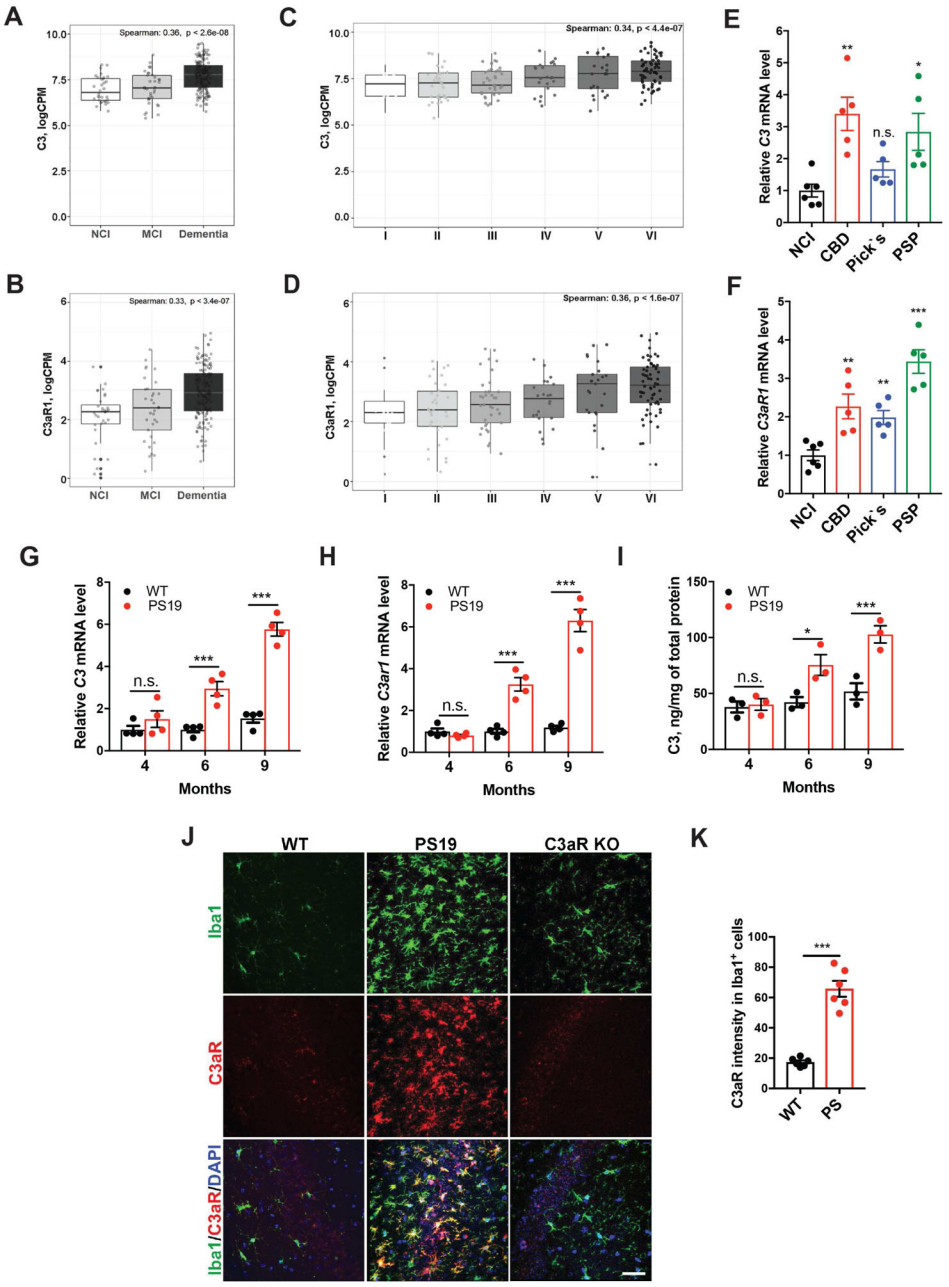

Figure 1. Upregulation of C3 and C3aR in AD and tauopathy conditions.

(A, B) *C3* (A) and *C3aR1* (B) mRNA levels in the parahippocampal gyrus of NCI (n=32), MCI (n=34), or AD (Dementia, n=160). Spearman's correlation, ρ (C3)=0.36, p<2.6E-08; ρ (C3aR)=0.33, p<3.4E-07.

(C, D) Positive correlation of *C3* (C) and *C3aR1* (D) mRNA levels with Braak scores (from I to VI: n(I)=24, n(II)=34, n(III)=37, n(IV)=22, n(V)=25, n(VI)=62). Spearman's correlation, ρ (C3)=0.34, p<4.4E-07; ρ (C3aR)=0.36, p<1.6E-07. Data used for A-D are from the Mount Sinai datasets available at the AMP-AD portal (Syn8484987).

(E, F) qPCR analysis of *C3* (E) and *C3aR*1 (F) mRNA levels in MFC of human tauopathy brain samples (mean ± s.e.m). NCI (n=6), CBD (n=5), Pick `s disease (n=5), PSP (n=5).

One-way ANOVA followed by Sidak ` s HSD test. n.s.: non-significant; *ρ<0.05; **ρ<0.01; ***ρ<0.001.

(G, H) qPCR analysis of *C3* (G) and *C3ar1* (H) mRNA levels in 4, 6 and 9 month-old wild-type (WT) and PS19 mice (mean ± s.e.m). n=4/genotype/age. Two-way ANOVA followed by Sidak ` s HSD test. n.s.: non-significant; ***ρ<0.001.

(I) ELISA analysis of C3 protein levels in brain samples of 4, 6 and 9 month-old WT and PS19 mice (mean ± s.e.m). n=3/genotype/age. Two-way ANOVA followed by Sidak ` s HSD test. n.s.: non-significant; *ρ<0.05; ***ρ<0.001.

(J) Representative co-immunostaining of C3aR1 and Iba1 with DAPI in the hippocampus of 9 month-old WT and PS19 mice. C3aR KO is used as a negative control. Scale bar: 50 μM.

(K) Quantification of (J) (mean ± s.e.m). n=6/genotype. Student ` s t-test. ***ρ<0.001.

See also Figure S1.

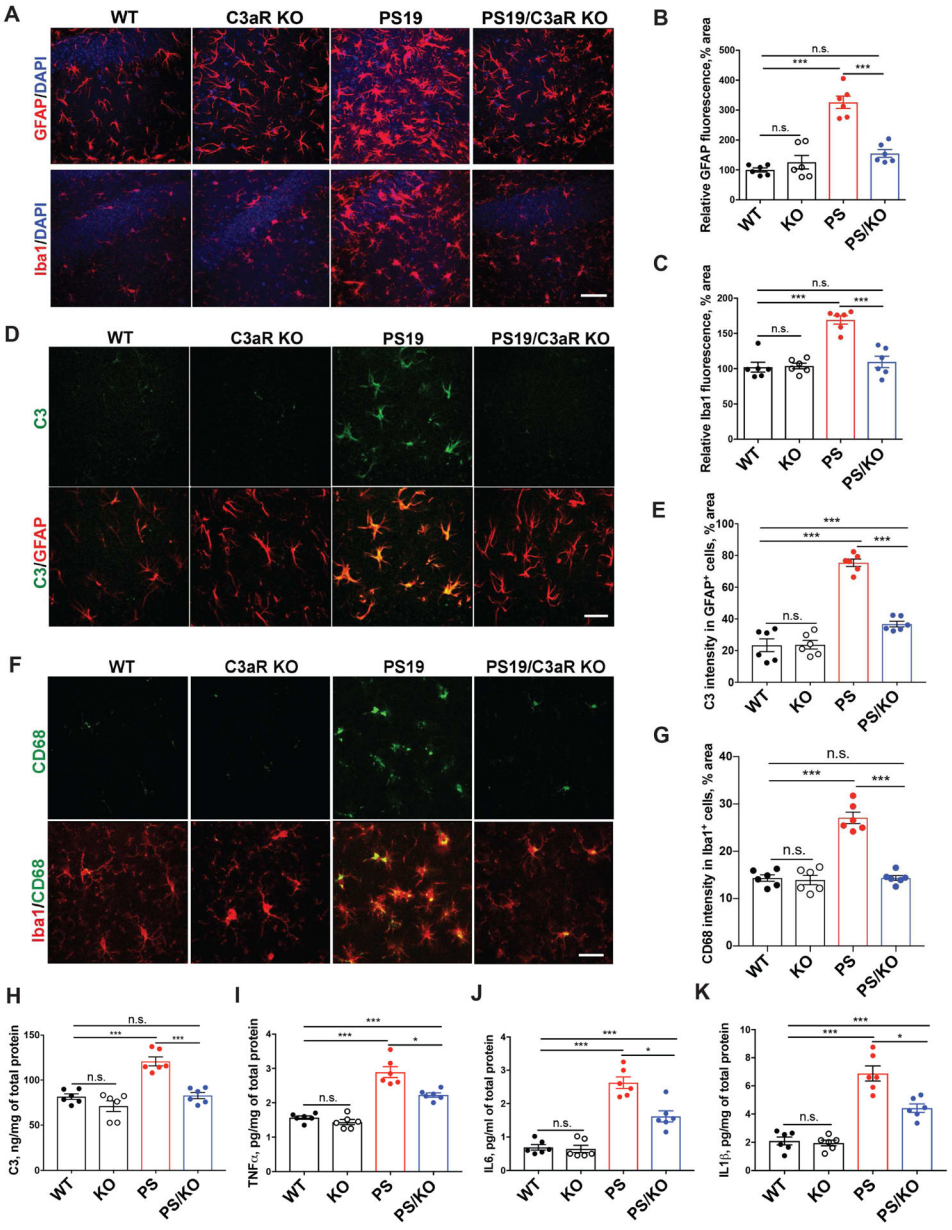

Figure 2. Genetic deletion of *C3ar1* attenuates reactive gliosis and neuroinflammation in PS19 mice.

(A)Representative GFAP and Iba1 immunostainings with DAPI in the hippocampus of 9 month-old WT, C3aR KO, PS19, and PS19/C3aR KO mice. Scale bar: 50 μM.

(B, C) Quantification of GFAP (B) and Iba1 (C) immunoreactivities (mean ± s.e.m). n=6 mice/genotype. One-way ANOVA followed by Sidak ` s HSD test. n.s.: non-significant; ***p<0.001.

(D)C3 and GFAP co-immunostaining in the hippocampus of 9 month-old WT, C3aR KO, PS19, and PS19/C3aR KO mice. Scale bar: 25 μM.

(E)Quantification of (D) (mean ± s.e.m). n=6 mice/genotype. One-way ANOVA followed by Sidak ` s HSD test. n.s.: non-significant; ***p<0.001.

(F) CD68 and Iba1 co-immunostaining in the hippocampus of 9 month-old WT, C3aR KO, PS19, and PS19/C3aR KO mice. Scale bar: 25 μM.
(G) Quantification of (E) (mean ± s.e.m). n=6 mice/genotype. One-way ANOVA followed by Sidak ` s HSD test. n.s.: non-significant; ***p<0.001.
(H-K) C3 (H), TNFα (I), IL6 (J) and IL 1β (K) protein levels in 9 month-old WT, C3aR KO, PS19, and PS19/C3aR KO mouse brains measured by ELISA (mean ± s.e.m). n=6/genotype for all experiments. One-way ANOVA followed by Sidak ` s HSD test. n.s.: non-significant; *p<0.05; ***p<0.001.
See also Figure S2.

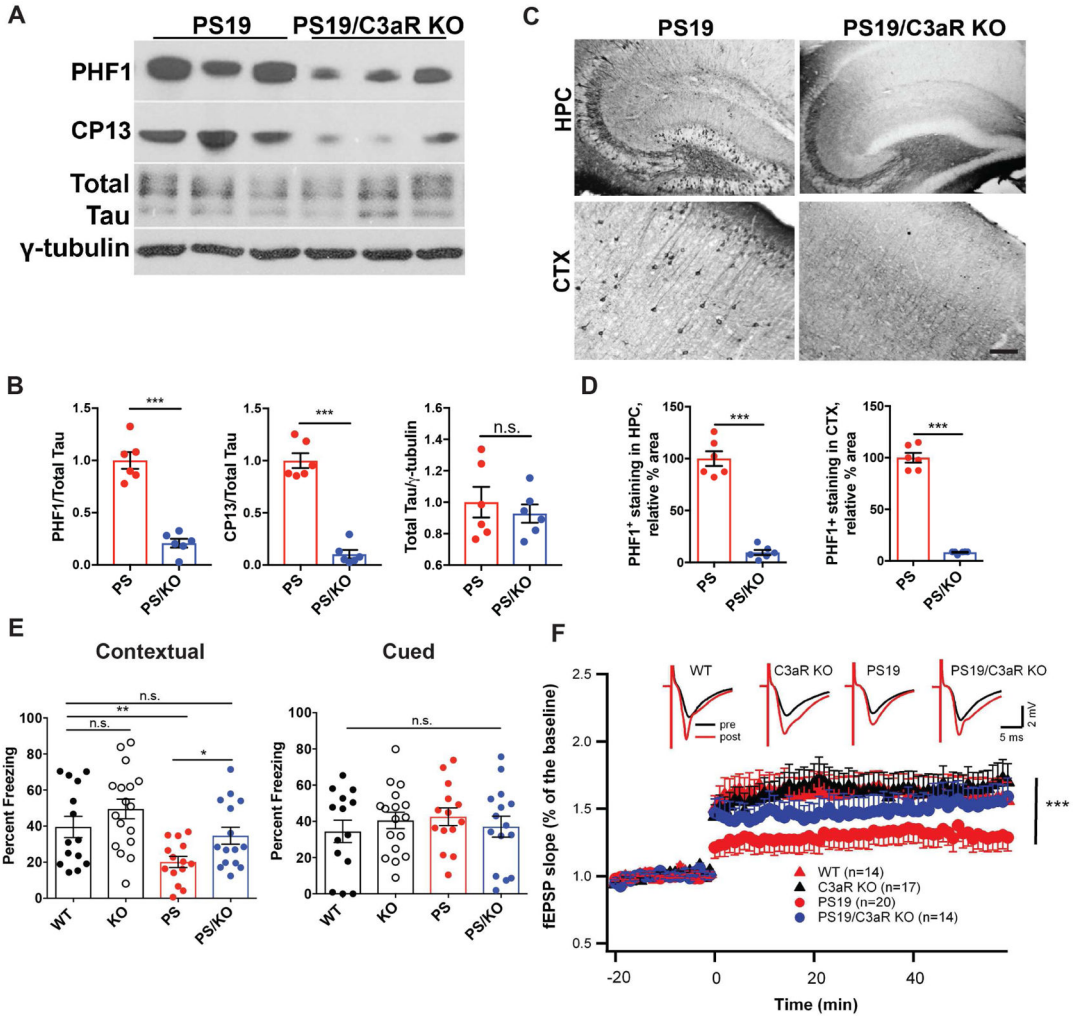

Figure 3. Genetic deletion of *C3ar1* reduces tau pathology and rescues behavioral deficits in PS19 mice.

(A) Representative Western blots of PHF1- and CP13-positive phospho-tau and total tau in PS19 and PS19/C3aR KO mouse brains at 9 months. γ-tubulin is used as a loading control.

(B) Quantification (A) (mean ± s.e.m). n=6/genotype. Student ` s t-test. n.s.: non-significant; ***p<0.001.

(C) Representative PHF1 immunohistochemical staining in hippocampus (HPC) and cortex (CTX) of 9 month-old PS19 and PS19/C3aR KO mice. Scale bar: 0.5 mm.

(D) Quantification of (C) (mean ± s.e.m). n=6/genotype. Student ` s t-test. ***p<0.001.

(E) Contextual (left) and cued (right) fear conditioning test performed in 8 month-old wild-type (WT, n=14), C3aR KO (KO, n=17), PS19 (PS, n=14), and PS19/C3aR KO (PS/KO, n=15) mice. One-way ANOVA followed by Sidak ` s HSD test. n.s.: non-significant; *p<0.05; **p<0.01. Data shown is mean ± s.e.m.

(F) Slope of field excitatory postsynaptic potential (fEPSP) in response to theta burst stimulation delivered to the Schaffer collateral pathway from WT, C3aR KO, PS19, and PS19/C3aR KO mice. Top: example fEPSP traces taken before (blue) or after (red) stimulation. Calibration: 2 mV, 5 msec. n=number of slices per genotype. Two-way repeated

measures ANOVA (between groups) followed by Tukey ` s HSD test. ***$p<0.001$. Data shown is mean ± s.e.m.
See also Figure S3.

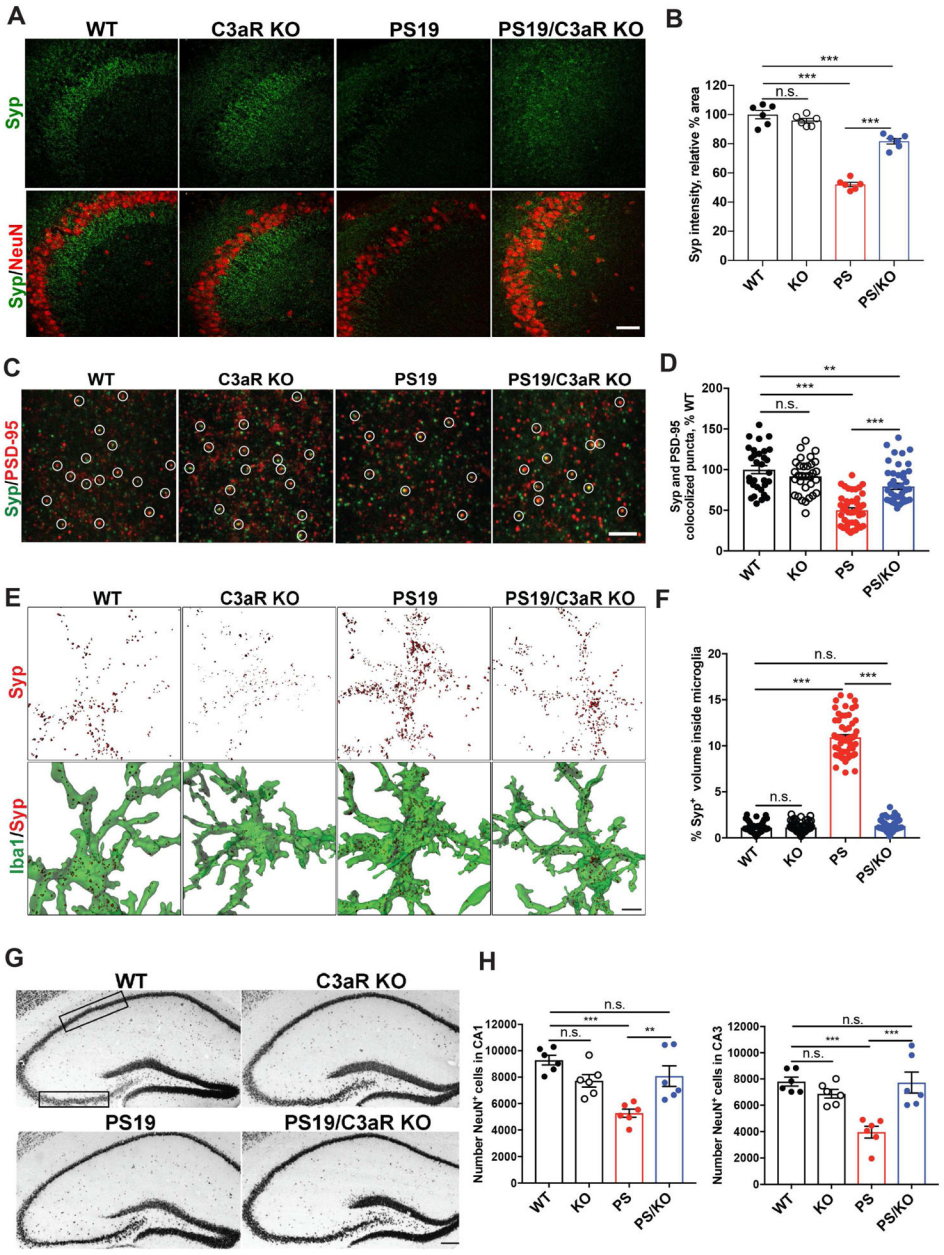

Figure 4. Genetic deletion of *C3ar1* rescues synaptic deficits and neurodegeneration in PS19 mice.

(A) Representative synaptophysin (Syp) and Syp/NeuN co-immunostaining in area CA3 of hippocampus of WT, C3aR KO, PS19, and PS19/C3aR KO mice at 9 months. Scale bar: 50 μM.

(B) Quantification of (A) (mean ± s.e.m). n=6/genotype. One-way ANOVA followed by Sidak ` s HSD test. n.s.: non-significant; ***p<0.001.

(C) Representative high magnification confocal images of Syp and PSD-95 co-immunostaining in area CA3 of hippocampus of WT, C3aR KO, PS19, and PS19/C3aR KO mice at 9 months. Colocolized punctas are marked by circles. Scale bar: 5 μM.

(D) Quantification of (C) (mean ± s.e.m). n=6/genotype with 5-7 planes per mouse. One-way ANOVA followed by Sidak ` s HSD test. n.s.: non-significant; **p<0.01; ***p<0.001.
(E) Representative 3D reconstruction and rendering of Syp signals inside Iba1-positive microglia (Iba1/Syp) from WT, C3aR KO, PS19, and PS19/C3aR KO mice at 9 months using the Imaris software. Scale bar: 5 μM.
(F) Quantification of (E) (mean ± s.e.m). n=6/genotype; 10-15 cells/mouse were quantified. One-way ANOVA followed by Sidak ` s HSD test. n.s.: non-significant; ***p<0.001.
(G) Representative NeuN immunohistochemical staining in hippocampus of 9 month-old WT, C3aR KO, PS19, and PS19/C3aR KO mice. Rectangles mark CA1 (upper) and CA3 (lower) areas selected for quantification. Scale bar: 0.5 mm.
(H) Estimate of neuronal numbers in CA1 (left) and CA3 (right) using unbiased stereology. n=6/genotype; three equidistant planes separated by 150 μM per animal. One-way ANOVA followed by Sidak ` s HSD test. n.s.: non-significant; **p<0.01; ***p<0.001.
See also Figure S3.

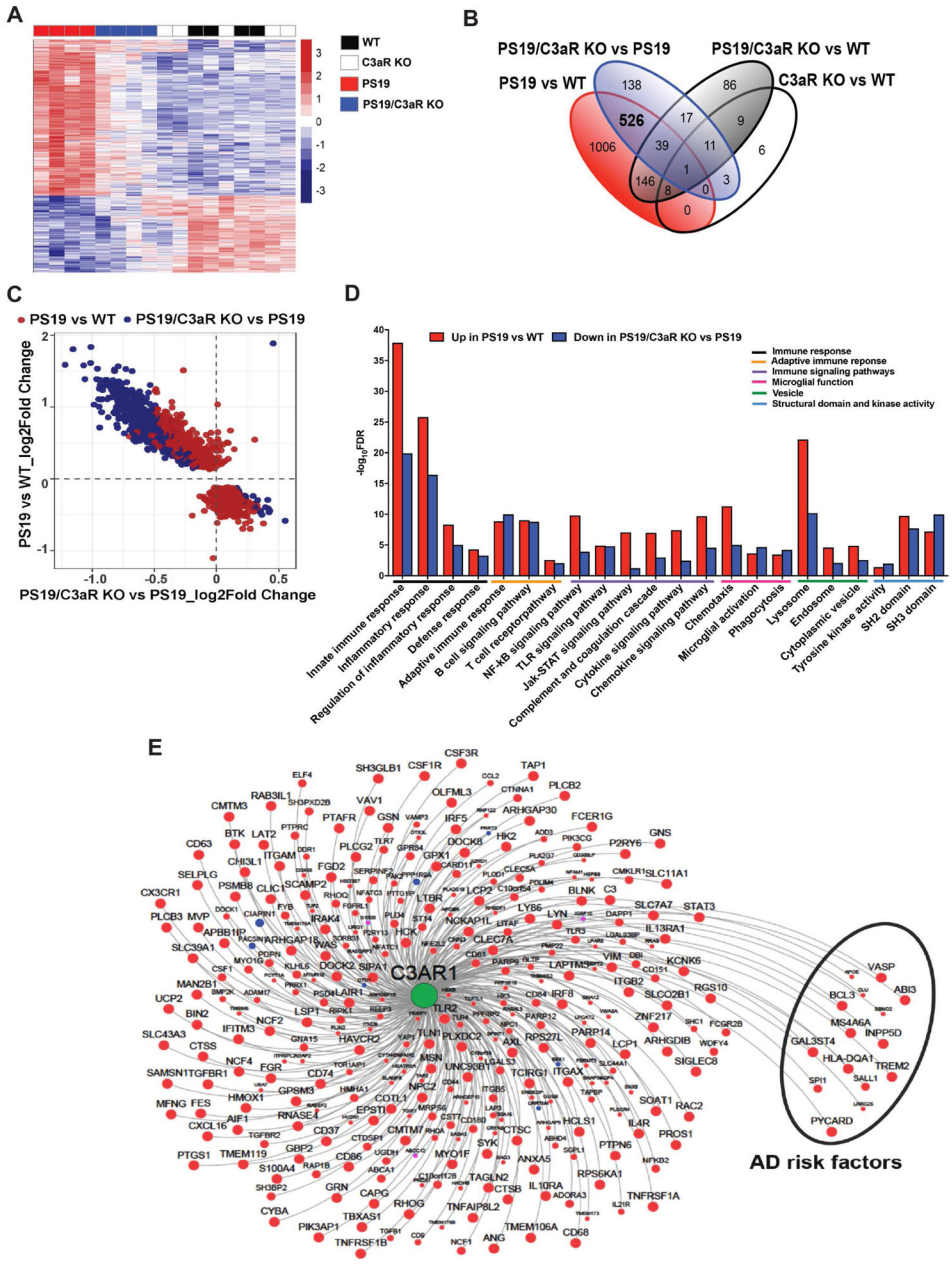

Figure 5. C3aR regulates the expression of immune pathway genes in PS19 mice conserved in human AD.

(A) Unsupervised clustering gene expression heatmap from RNAseq analysis of hippocampal tissues of 9 month-old WT, C3aR KO, PS19, and PS19/C3aR KO mice. 1726 DEGs were identified by comparing the PS19 vs WT group (1155 genes upregulated, red, and 571 downregulated, blue). n=4-5/genotype, adjusted $p<0.01$.

(B) Venn diagram with number of DEGs identified in four comparisons: PS19 vs WT (red circle); PS19/C3aR KO vs PS19 (blue circle); PS19/C3aR KO vs WT (grey circle) and C3aR KO vs WT (unfilled circle). The 526 genes rescued by C3aR KO (significant between PS19/C3aR KO vs PS19 and insignificant between PS19/C3aR KO vs WT) are highlighted in bold.

(C) Comparison of expression changes between PS19 vs WT (y-axis) and PS19/C3aR KO vs PS19 (x-axis) showing that the 526 genes rescued by C3aR KO (blue) are predominately clustered within the upregulated DEGs in PS19 vs WT (red, n=499) in the upper left quadrant.

(D) Gene Ontology analysis of the 1155 upregulated genes in PS19 vs WT comparison (red) and the 499 upregulated genes rescued by C3aR KO (blue).

(E) A *C3AR1*-centered network confirmed in both human AD brain studies (using consensus *C3AR1*-correlated gene signatures) and PS19/C3aR KO mice. Genes within this network significantly correlate with *C3AR1* expression in at least five human AD datasets (MSSM BM10, 22, 36, 44; HBTRS PFC, VC, CR; ROS-MAP). The node size is proportional to the number of datasets in which a particular gene significantly correlates with *C3AR1* expression. Red nodes represent genes that are positively correlated with *C3AR1* in human AD studies and are downregulated in PS19/C3aR KO mice (n=301). Blue nodes represent the genes negatively correlated with *C3AR1* in human AD datasets and upregulated in PS19/C3aR KO mice (n=7). Pink nodes represent the genes negatively correlated with *C3AR1* in human AD datasets but not upregulated in PS19/C3aR KO mice (n=3). Human AD risk factors correlated with *C3AR1* expression are as indicated.

See also Figure S4.

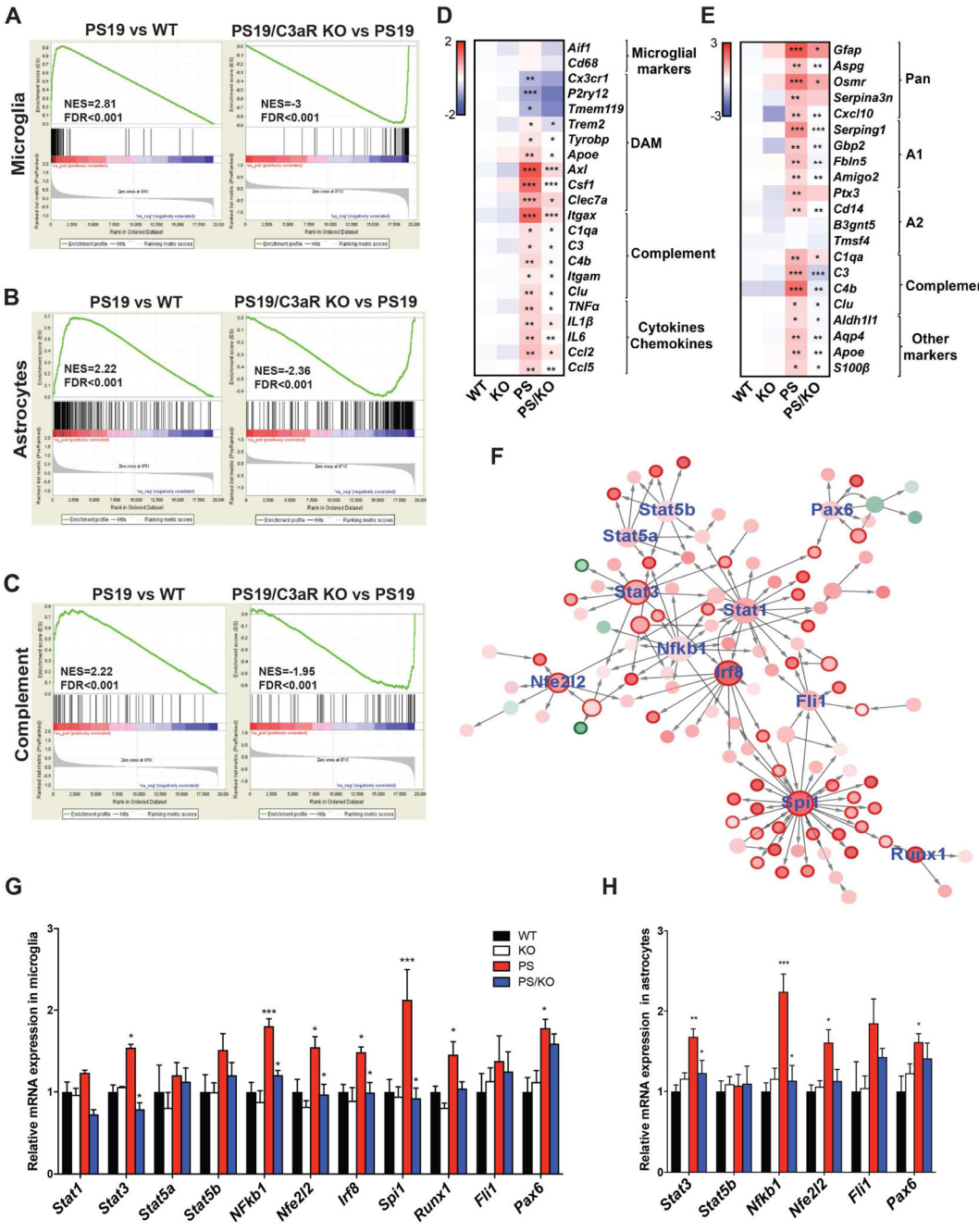

Figure 6. C3aR signaling activates the inflammatory and microglia proliferation transcription factors in PS19 mice.

(A) Gene-set enrichment analyses (GSEA) of the microglia sensome gene list in PS19 vs WT (left, NES=2.81, FDR<0.001) and in PS19/C3aR KO vs PS19 (right, NES= −3.0, FDR<0.001) comparisons. NES: normalized enrichment score; FDR: false discovery rate.

(B) GSEA of the reactive astrocyte gene list in PS19 vs WT (NES=2.22, FDR<0.001) and in PS19/C3aR KO vs PS19 (NES = −2.36, FDR<0.001) comparisons.

(C) GSEA of the complement pathway gene list in PS19 vs WT (NES=2.22, FDR<0.001) and in PS19/C3aR KO vs PS19 (ES= −1.95, FDR<0.001) comparisons.

(D, E) qPCR analysis of mRNA expression in CoBrA-isolated microglia (D) and astrocytes (E) from WT, C3aR KO, PS19, and PS19/C3aR KO mice. The asterisks in PS19 column represent the comparison between PS19 and WT, and in PS19/C3aR KO represent the comparison between PS19/C3aR KO and PS19. n=6/genotype. Two-way ANOVA followed by Tukey's HSD test. *p<0.05; **p<0.01; ***p<0.001.

(F) Transcription factor network analysis of the 1726 DEGs in PS19 vs WT mice generated using the TRANSFAC database. Hub genes in the network denote the TFs that regulate the transcription of DEGs in PS19. Other network nodes represent the TFs' downstream targets. The size of the node corresponds to the number of gene connections while the color intensity represents the degree of changes comparing PS19 vs WT (red: upregulated; green: downregulated). Genes rescued in PS19/C3aR KO are highlighted by a dark red circle around the node.

(G, H) qPCR analysis of hub gene expression levels in CoBrA-isolated microglia (G) and astrocytes (H). The asterisks above PS19 represent the PS19 vs WT comparison and those above PS19/C3aR KO is for PS19 vs PS19/C3aR KO comparison. n=6/genotype. Student `s t-test. *p<0.01; **p<0.01; ***p<0.001. All data is presented as mean ± s.e.m.

See also Figures S5-S7.

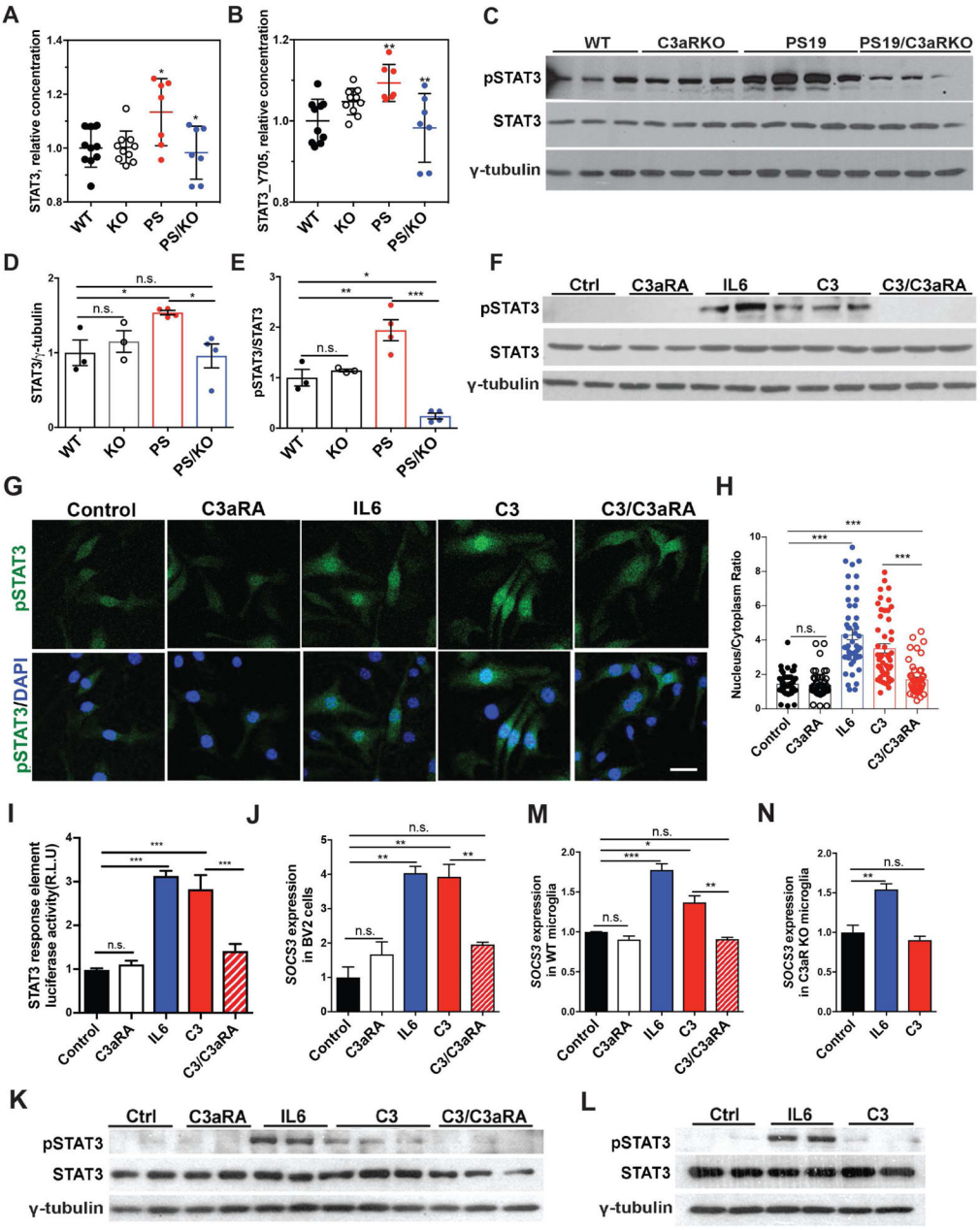

Figure 7. Direct regulation of STAT3 phosphorylation and signaling by C3-C3aR.

(A, B) Total STAT3 (A) and Y705-phospho-STAT3 (B) levels in 9 month-old WT (n=10), C3aR KO (KO, n=10), PS19 (PS, n=7), and PS19/C3aR KO (PS/KO, n=7) mice measured by RPPA (mean ± s.e.m). The asterisks above PS19 are for PS19 vs WT comparison; those above PS19/C3aR KO are for PS19/C3aR KO vs PS19 comparison. Student ` s t-test. *p<0.05; **p<0.01.

(C) Western blots of total- and phospho-STAT3 (pSTAT3) in 9 month-old WT, C3aR KO, PS19, and PS19/C3aR KO mice. γ-tubulin is used as a loading control.

(D, E) Quantification of total STAT3/ γ-tubulin (D) and pSTAT3/STAT3 (E) levels. n=3-4/ genotype. One-way ANOVA followed by Sidak ` s HSD test. n.s.: non-significant; *p<0.05; **p<0.01; ***p<0.001.

(F) Representative Western blots of pSTAT3 and STAT3 in BV2 cells treated with vehicle control (Ctrl), C3aR antagonist (C3aRA, 100 uM), IL6 (50 nM), C3 (100 nM) or C3 plus C3aRA (C3/C3aRA). γ-tubulin is used as a loading control..

(G) Representative pSTAT3 immunostaining with or without DAPI in BV2 cells with the same treatment as (F). Scale bar: 20 μM.

(H) Quantification of nuclear/cytoplasmic pSTAT3. n=50 cells/treatment. One-way ANOVA followed by Sidak ` s HSD test. n.s.: non-significant; ***p<0.001..

(I) Relative luciferase activity in BV2 cells infected with the luciferase reporter driven by the STAT3 response element and with the same treatment as (F). One-way ANOVA followed by Sidak ` s HSD test. n.s.: non-significant; ***p<0.001.

(J) qPCR analysis of *SOCS3* mRNA levels in BV2 cells with the same treatment as (F). Oneway ANOVA followed by Sidak ` s HSD test. n.s.: non-significant; **p<0.01.

(K) Representative Western blots of pSTAT3 and STAT3 in primary WT microglial cultures treated with vehicle (Ctrl), C3aRA, IL6, C3 or C3 plus C3aRA. γ-tubulin is used as a loading control.

(L) Representative Western blot analysis of pSTAT3 and STAT3 in primary microglial cultures derived from C3aR KO mice treated with Ctrl, IL6, or C3. γ-tubulin is used as a loading control.

(M, N) qPCR analysis of *SOCS3* mRNA levels in primary WT (M) or C3aR KO (N) microglial cultures with treatments as indicated. One-way ANOVA followed by Sidak ` s HSD test. n.s.: nonsignificant; *p<0.05; **p<0.01; ***p<0.001.

All data is presented as mean ± s.e.m. All cell culture experiments were repeated three to four times each in triplicates.

See also Figure S8.

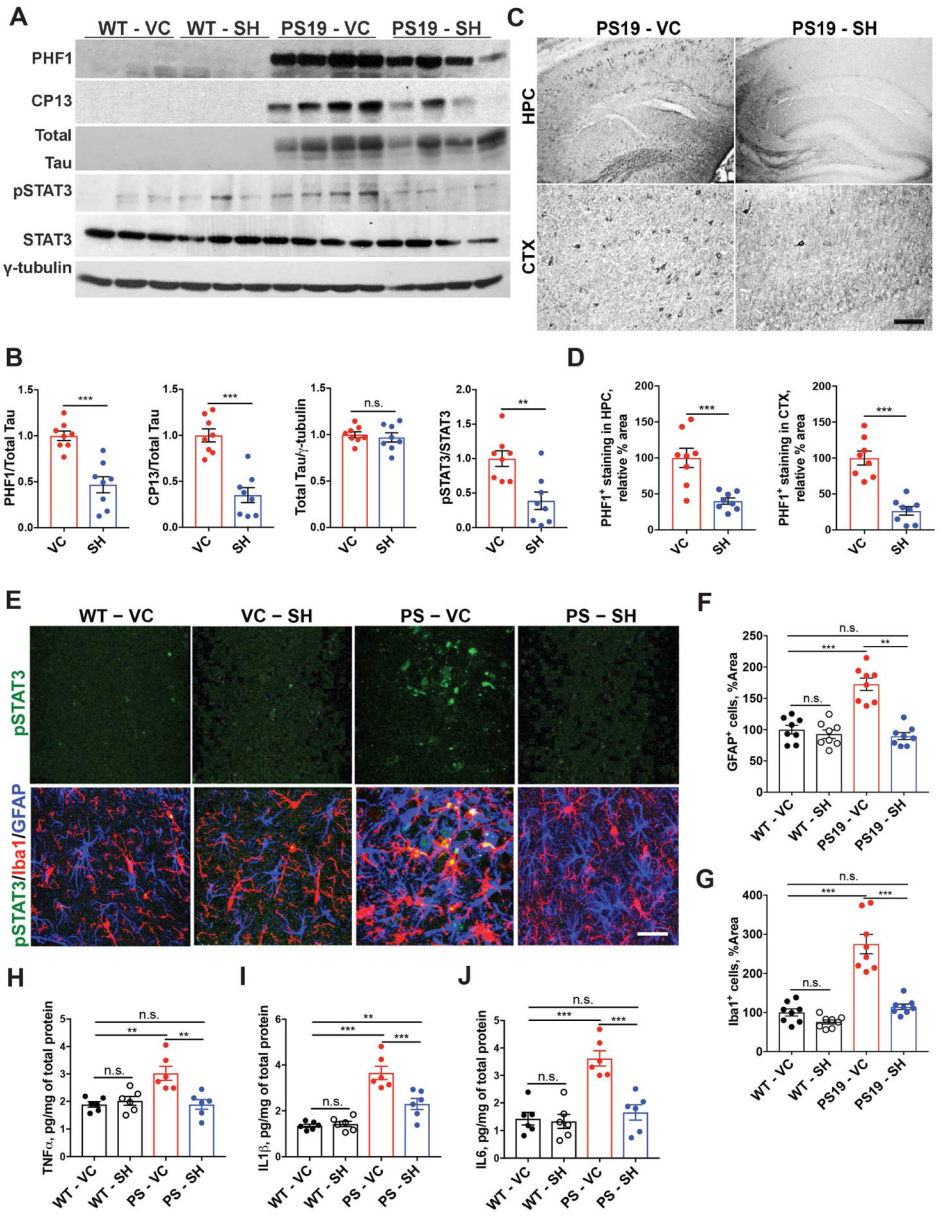

Figure 8. STAT3 inhibitor treatment mitigates tau pathology and neuroinflammation in aged PS19 mice.

(A) Representative Western blots using PHF1 and CP13 phospho-tau antibodies and antibodies against total tau, pSTAT3 and total STAT3 in brain samples of WT and PS19 mice treated with vehicle control (VC) or SH-4-54 (SH, 10 mg/kg) starting at 7 months for 2 months. γ-tubulin is used as a loading control.

(B) Quantification of (A) (mean ± s.e.m). n=8/genotype. Student ` s t-test. n.s.: non-significant; ** p<0.01; *** p<0.001.

(C) Representative PHF1 immunohistochemical staining in the hippocampus (HPC) and cortex (CTX) of vehicle (VC) or SH-treated PS19 mice. Scale bar: 0.5 mm.

(D) Quantification of (C). n=8/genotype. Student ` s t-test. *** p<0.001.

(E) Representative pSTAT3, GFAP and Iba1 co-immunostainings in HPC of WT or PS19 mice treated with VC or SH. Scale bar: 50 μM.

(F, G) Quantification of GFAP (F) and Iba1 (F) immunoreactivities in above treated mice. n=8/genotype/treatment. One-way ANOVA followed by Sidak ` s HSD test. n.s.: non-significant; ** $p<0.01$; *** $p<0.001$.

(H-J) TNFa (H), IL1 β (I), and IL6 (J) levels measured by ELISA in WT and PS19 mice treated with VC or SH. n=6/genotype/treatment. One-way ANOVA followed by Sidak ` s HSD test. n.s.: non-significant; ** $p<0.01$; *** $p<0.001$. All data is shown as mean ± s.e.m. See also Figure S8.